Production of DM associated to a Higgs decaying into two photons in the ATLAS experiment

Alvaro Lopez Solis

Laboratoire de Physique Nucléaire et des Hautes Énergies

Journées de Rencontres Jeunes
Chercheurs 2015

Outline

- Motivation
- EFT and simplified models
- Analysis and results from Run I
- Important performances
- Electromagnetic calorimeter
- Cross-talk studies
  - Calibration → Physics method

Motivation

- Dark matter is one of the open mysteries of science:
  - Its existence can be inferred from measurements in galactic clusters
    - Looking at their luminosity/mass ratio (Zwicky, 1937)
    - Gravitational lensing (1980's)
  - Galaxy measurements:
    - Rotational velocity profile of stars around galactic center (Andromeda galaxy, Hα line shifts , Vera Rubin and Kent Ford, 1970).
  - Cosmological measurements ($\Omega_{nbm}h^2$ = 0.1198 $\pm$ 0.0026 in the ΛCDM model **from PDG**)
    - CMB anisotropies
    - Large scale structure.
    - Supernovae Type Ia

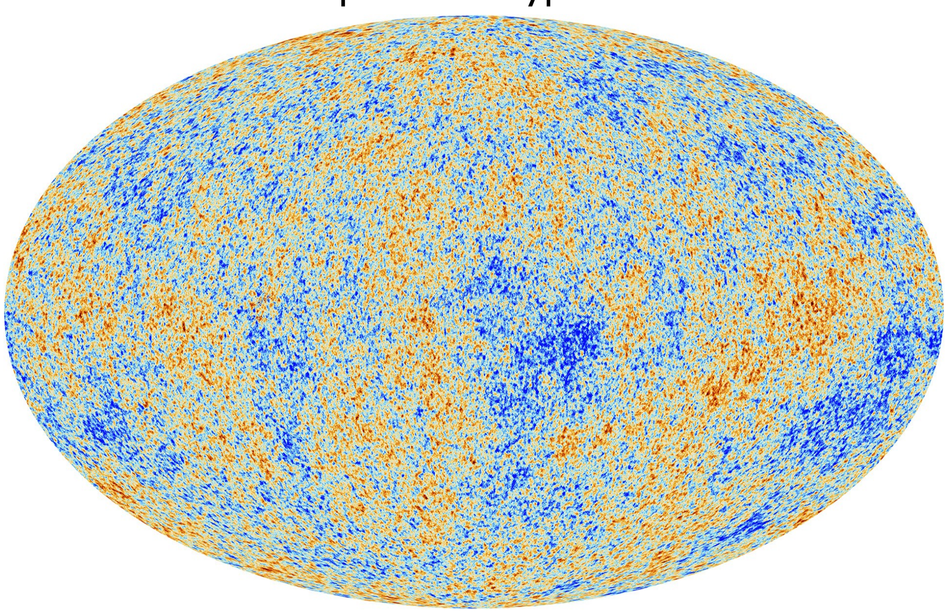

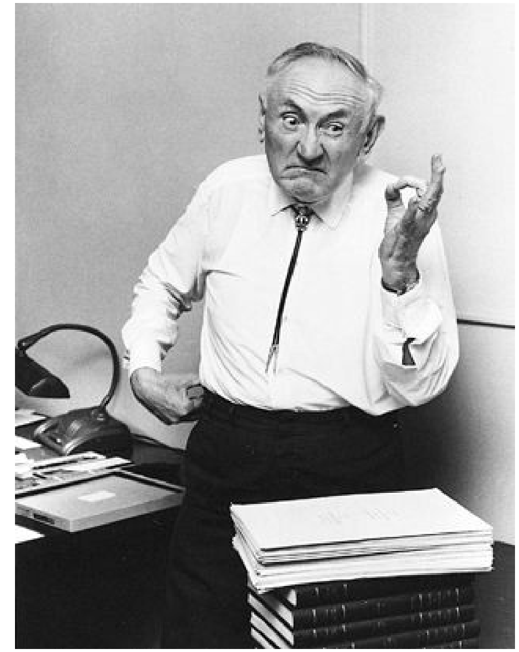

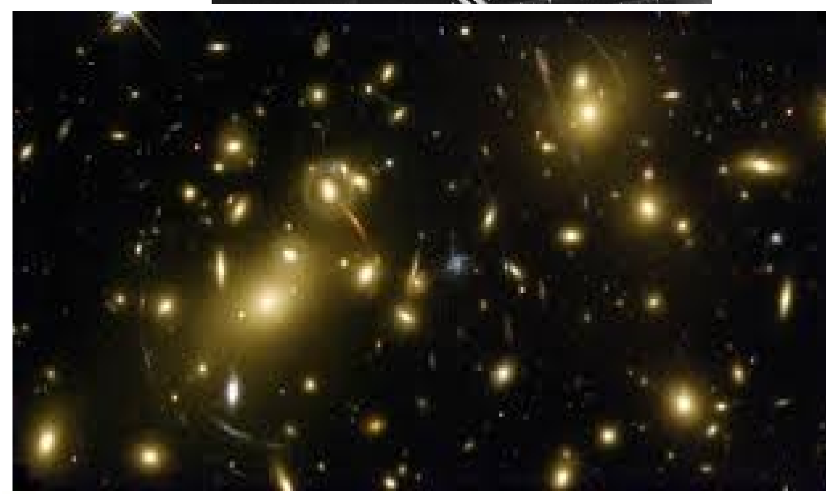

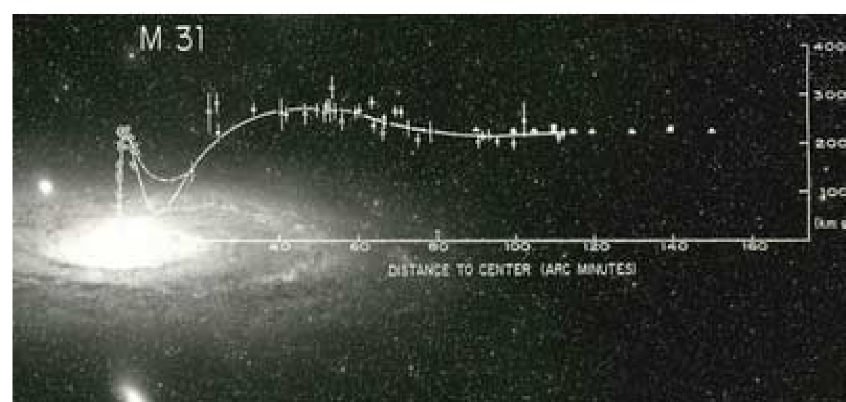

Motivation

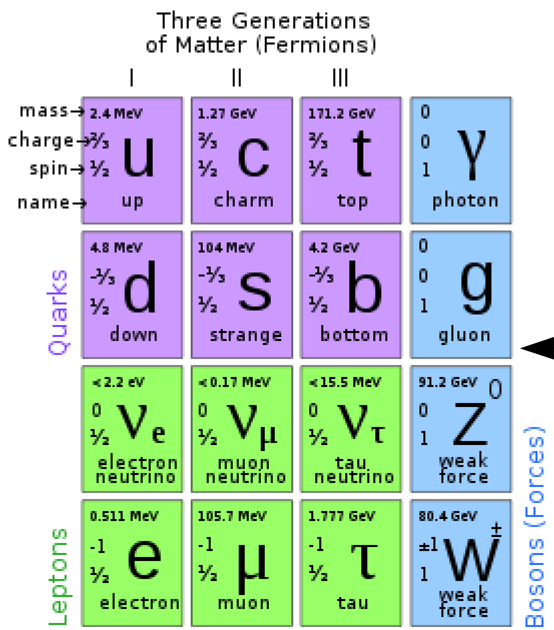

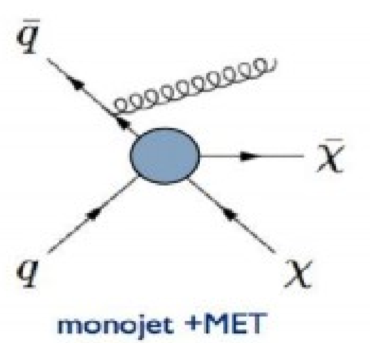

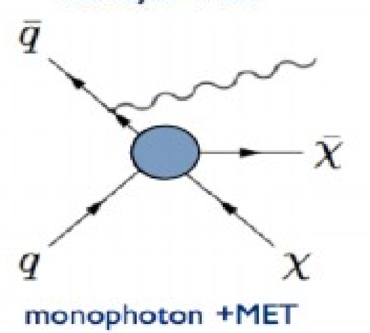

DM composition and interactions are still a mystery

No viable candidate in SM

Extensions introduce some DM candidates : LSP, sterile neutrino, axions etc

Focus on minimal extensions

Effective field theories (EFT) or simplified models.

Long range cosmology measurements favor that it is “cold” DM

Controversy at short range measurements → dwarf galaxies and halo substructure

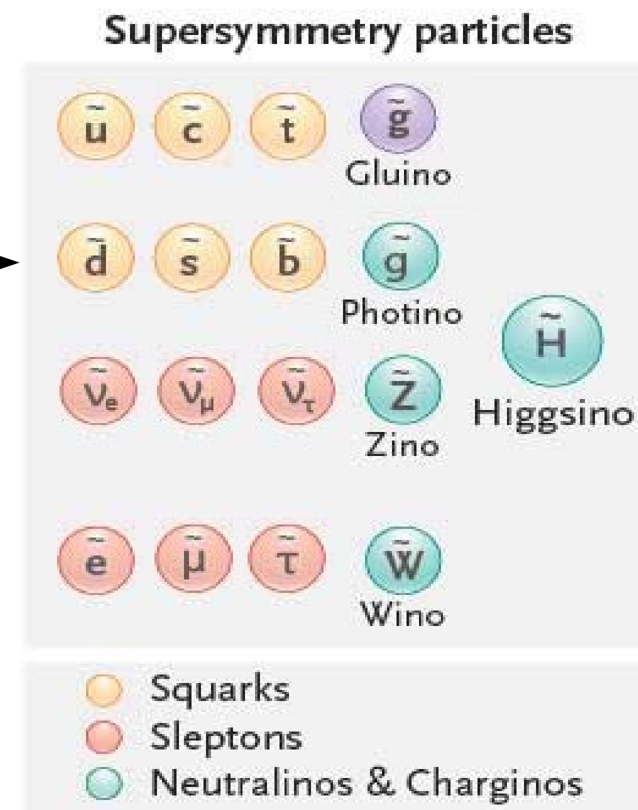

Motivation

DM composition and interactions are still a mystery

Long range cosmology measurements favor that it is “cold” DM

Controversy at short range measurements → dwarf galaxies and halo substructure

No viable

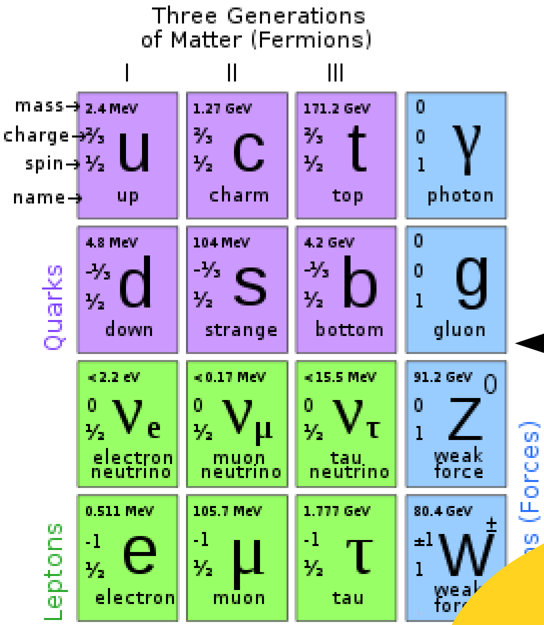

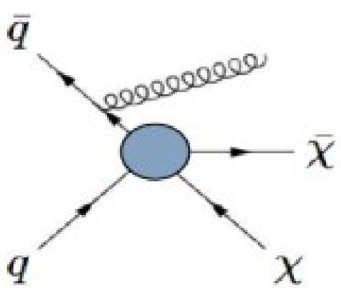

monojet +MET

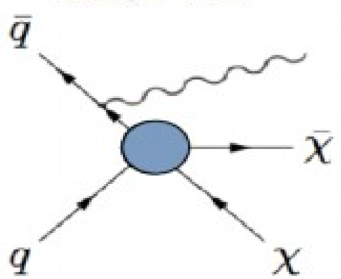

monophoton +MET

$H \rightarrow \gamma\gamma + E_T^{miss}$

...us on minimal extensions

Effective field theories (EFT) or simplified models.

EFT and simplified models

http://arxiv.org/abs/1312.2592

- **EFT theories:**
  - Mediator integrated out.
  - Parametrized by a Λ scale representing the UV domain integrated out → Non renormalizable.
  - Valid for $Q_{tr} < \Lambda$.
  - $Q_{tr} > 2m_{DM}$

Short Name	EFT Dimension	Operator	Parameters
xxhhs	4	$\lambda \lvert H \rvert^2 \chi\chi$	$\lambda,\ m_\chi$
xxhhg5	5	$\frac{1}{\Lambda} \lvert H \rvert^2 \bar{\chi} i \gamma_5 \chi$	$\Lambda,\ m_\chi$
xdxhDh	6	$\frac{1}{\Lambda^2} \chi^\dagger i \overleftrightarrow{\partial^\mu} \chi H^\dagger i D_\mu H$	$\Lambda,\ m_\chi$
xgxFhDh	8	$\frac{1}{\Lambda^4} \bar{\chi} \gamma^\mu \chi B_{\mu\nu} H^\dagger D^\nu H$	$\Lambda,\ m_\chi$

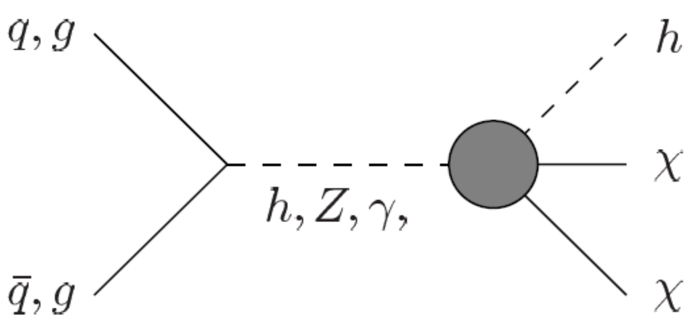

EFT and simplified models

http://arxiv.org/abs/1312.2592

- **EFT theories:**
  - Mediator integrated out.
  - Parametrized by a Λ scale representing the UV domain integrated out → Non renormalizable.
  - Valid for $Q_{tr} < \Lambda$.
  - $Q_{tr} > 2m_{DM}$

Short Name	EFT Dimension	Operator	Parameters
xxhhs	4	$\lambda\|H\|^2\chi\chi$	$\lambda,\ m_\chi$
xxhhg5	5	$\frac{1}{\Lambda}\|H\|^2\bar{\chi}i\gamma_5\chi$	$\Lambda,\ m_\chi$
xdxhDh	6	$\frac{1}{\Lambda^2}\chi^\dagger i \overleftrightarrow{\partial^\mu} \chi H^\dagger i D_\mu H$	$\Lambda,\ m_\chi$
xgxFhDh	8	$\frac{1}{\Lambda^4}\bar{\chi}\gamma^\mu\chi B_{\mu\nu}H^\dagger D^\nu H$	$\Lambda,\ m_\chi$

- **Simplified models:**
  - Hidden sector connected to SM by a vector boson or a scalar boson as mediators.
  - Vector boson → extend SM gauge → Gauge baryonic symmetry
  - Coupled to quarks and DM particles.

$$V \supset a|H|^2 S + b|H|^2 S^2 + \lambda_h |H|^4 - y_\chi \bar{\chi}\chi S$$

$$g_q \bar{q}\gamma^\mu q Z'_\mu + g_\chi \bar{\chi}\gamma^\mu \chi Z'_\mu$$

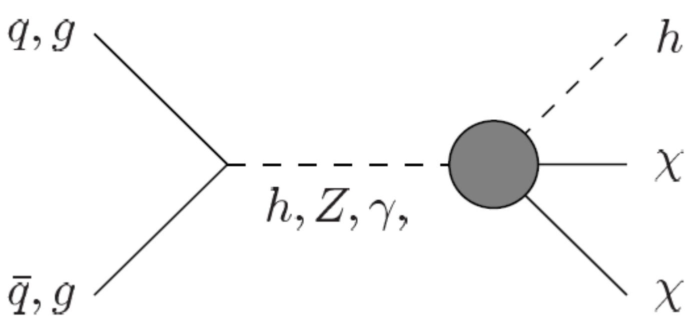

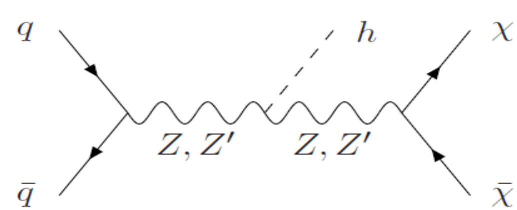

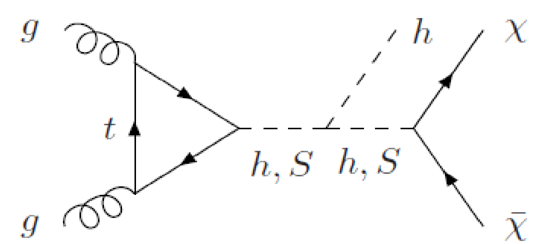

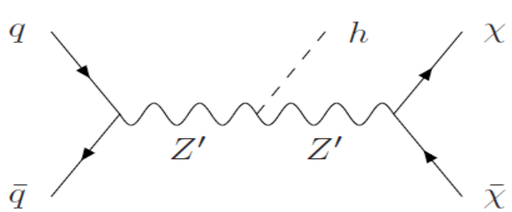

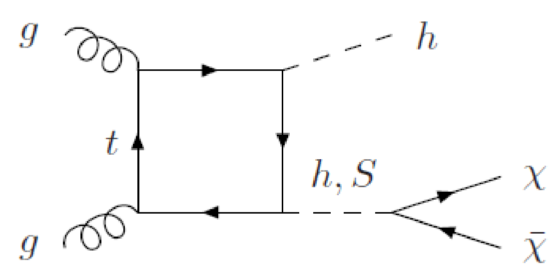

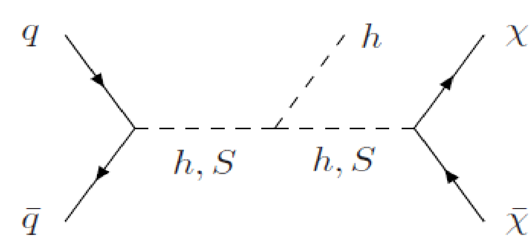

$H \rightarrow \gamma\gamma + E_T^{miss}$ analysis in Run I

http://arxiv.org/abs/1506.01081

- **Event selection**
  - $m_{\gamma\gamma} \in [105,160]$ GeV
  - Two final states photons pT > 25 GeV & |η| < 2.37
  - $p_T^{\gamma} > 0.35\ (0.25)\ m_{\gamma\gamma}$
  - $p_T^{\gamma\gamma} > 90$ GeV & $E_T^{miss} > 90$ GeV
- **Resonant background contributions**
  - **HZ & HW**
  - ggH, ttH and VBF production modes
- **Non resonant background**
  - **Wγγ, Zγγ** ($l\ \nu_l$ & $\nu\nu$)
  - **Wγ and Zγ** → One e^- misidentified as photon.
  - γγ+jets
  - $t\bar{t}$

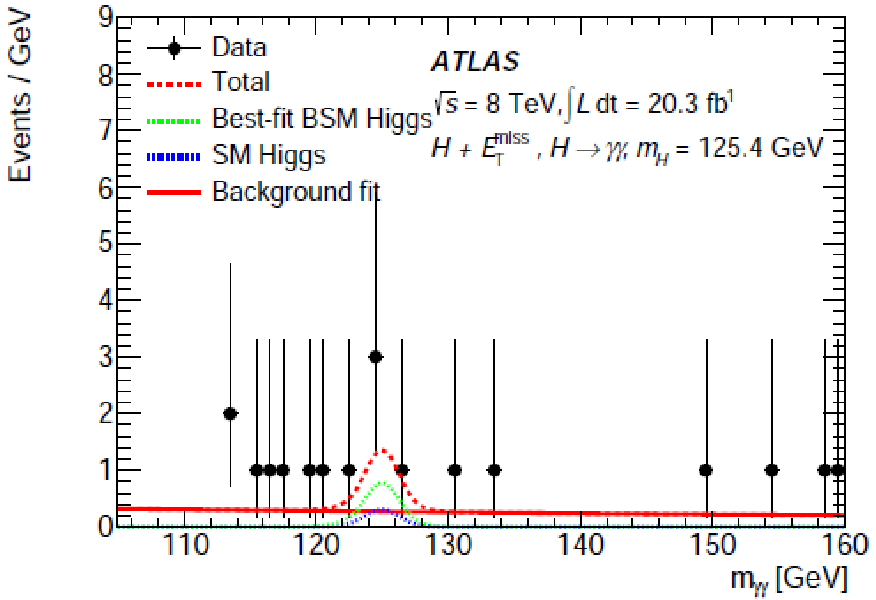

$H \rightarrow \gamma\gamma + E_T^{miss}$ analysis in Run I

http://arxiv.org/abs/1506.01081

- Event selection
  - $m_{\gamma\gamma} \in [105,160]$ GeV
  - Two final states photons pT > 25 GeV & $|\eta| < 2.37$
  - $p_T^{\gamma} > 0.35\ (0.25)\ m_{\gamma\gamma}$
  - $p_T^{\gamma\gamma} > 90$ GeV & $E_T^{miss} > 90$ GeV
- Resonant background contributions
  - HZ & HW
  - ggH, ttH and VBF production modes
- Non resonant background
  - $W\gamma\gamma$, $Z\gamma\gamma$ ($l\,\nu_l$ & $\nu\nu$)
  - $W\gamma$ and $Z\gamma$ → One e^- misidentified as photon.
  - $\gamma\gamma$+jets
  - $t\bar{t}$

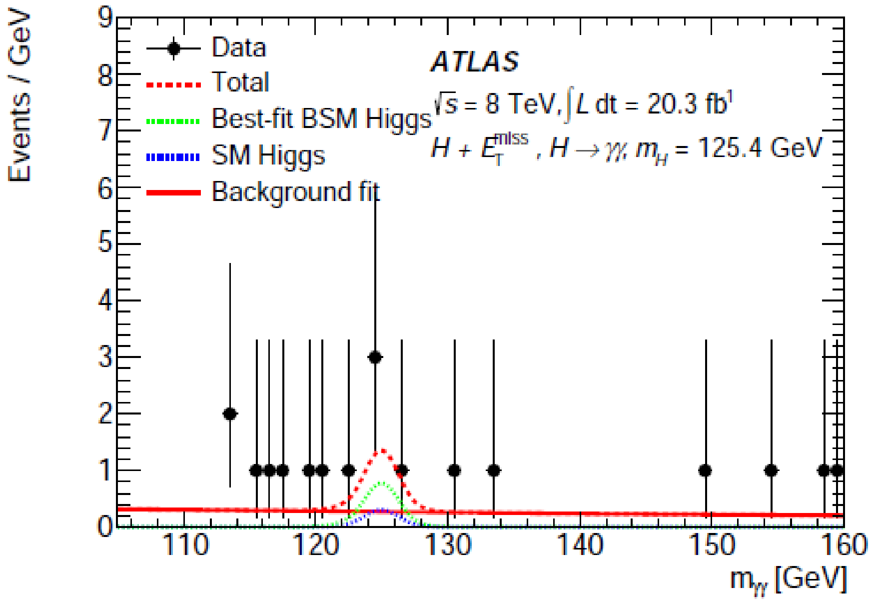

$H \rightarrow \gamma\gamma + E_T^{miss}$ analysis in Run I

http://arxiv.org/abs/1506.01081

- **Event selection**
  - $m_{\gamma\gamma} \in [105,160]$ GeV
  - Two final states photons pT > 25 GeV & |η| < 2.37
  - $p_T^{\gamma} > 0.35\ (0.25)\ m_{\gamma\gamma}$
  - $p_T^{\gamma\gamma} > 90$ GeV & $E_T^{miss} > 90$ GeV
- **Resonant background contributions**
  - **HZ & HW**
  - ggH, ttH and VBF production modes
- **Non resonant background**
  - **Wγγ, Zγγ** ($l\,\nu_l$ & νν)
  - **Wγ and Zγ** → One e^- misidentified as photon.
  - γγ+jets
  - $t\bar{t}$

Number of events observed in data represent **1.4 σ deviation from SM predictions.**

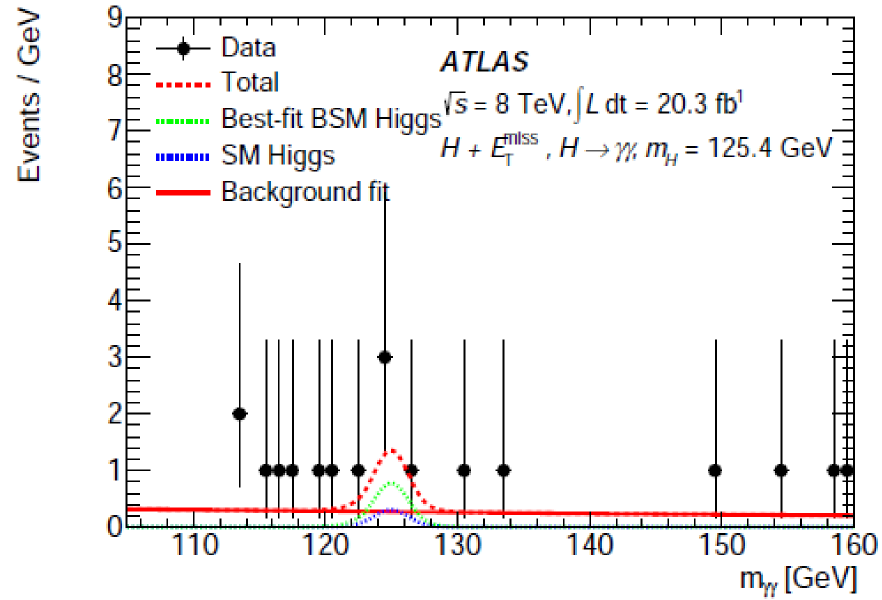

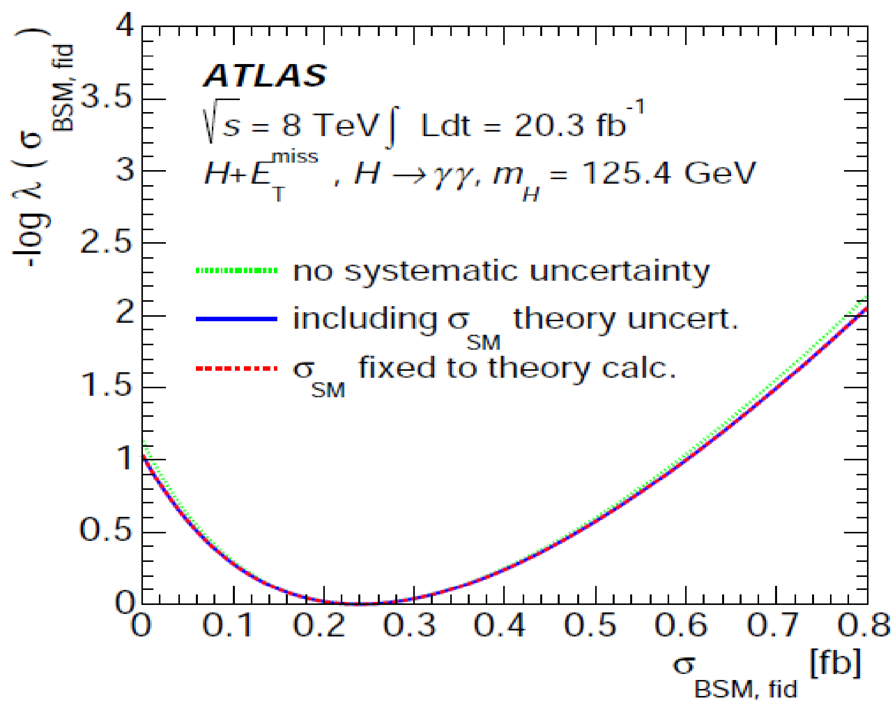

$H \rightarrow \gamma\gamma + E_T^{miss}$ analyses interpretation

http://arxiv.org/abs/1506.01081

Limits to EFT:

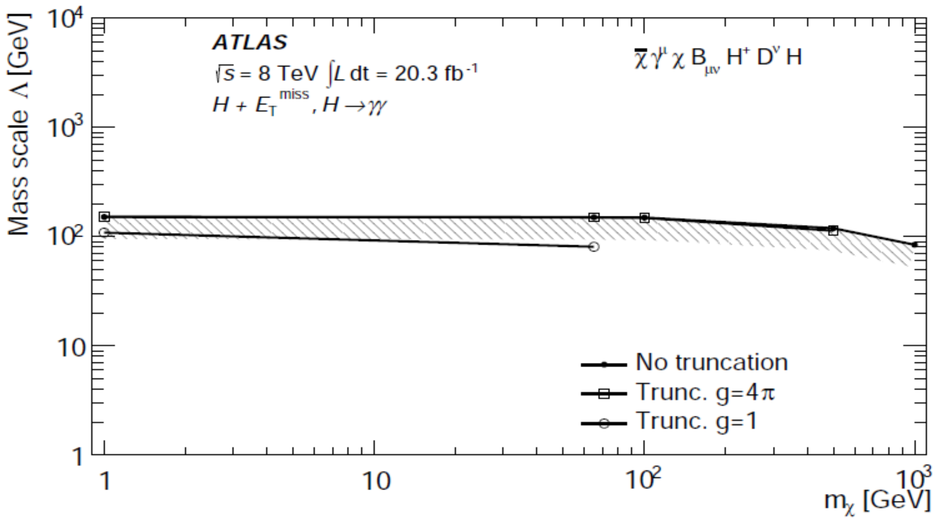

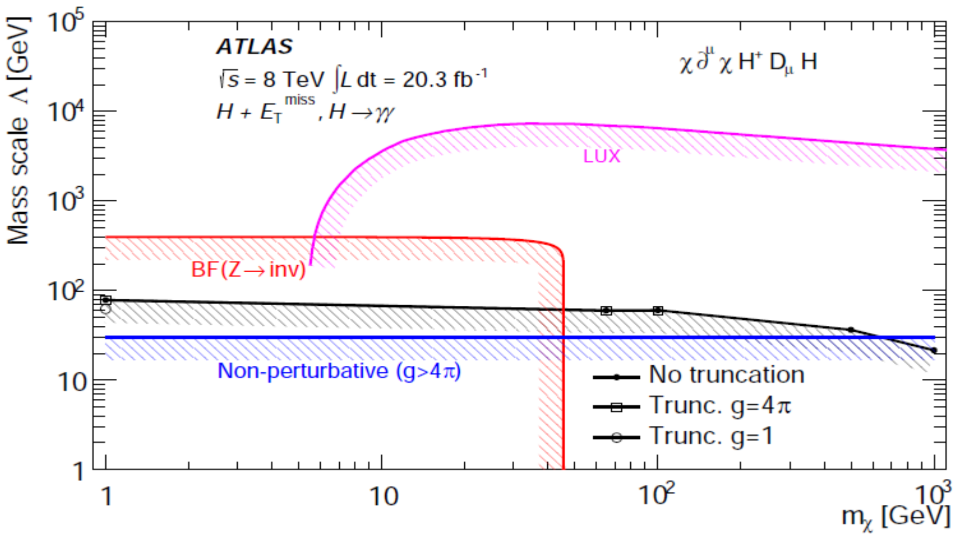

Limits to simplified models

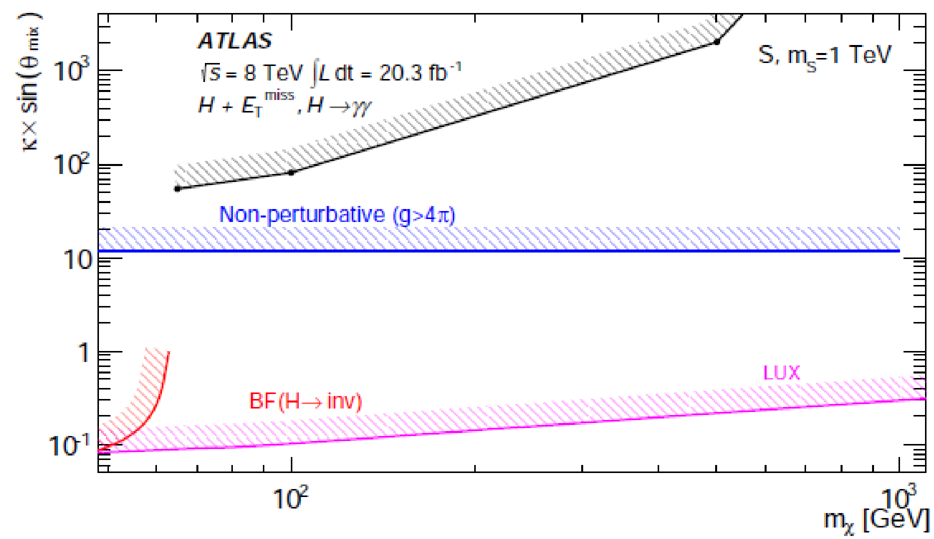

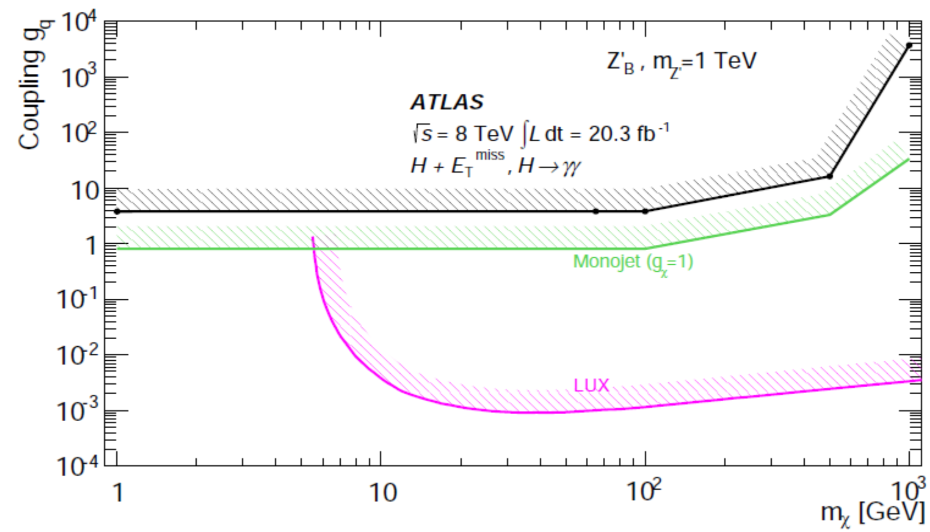

H → γγ + E_T^{miss} : a performance driven channel

http://arxiv.org/pdf/1207.7214v2.pdf

http://arxiv.org/pdf/1406.3827.pdf

Photon reconstruction and identification

- Photon clusters :
  - Cluster energy is the sum of cell energies in a Δη X Δϕ region.
  - Cluster shape → shower shapes
- Shower shape → photon identification (Pierre's talk)
  - Precisely measured by highly segmented calorimeter.
  - Reject jets from e/γ

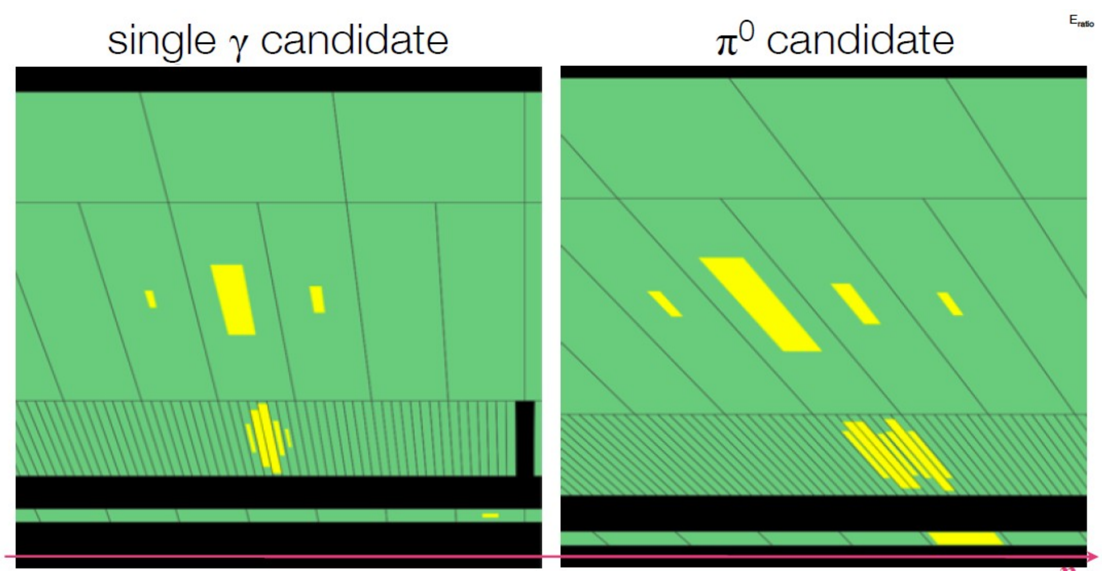

Di-photon pair invariant mass reconstruction

- Improvements on the photon energy reconstruction and identification

→ Improve resolution of Higgs peak and remove a part of the background

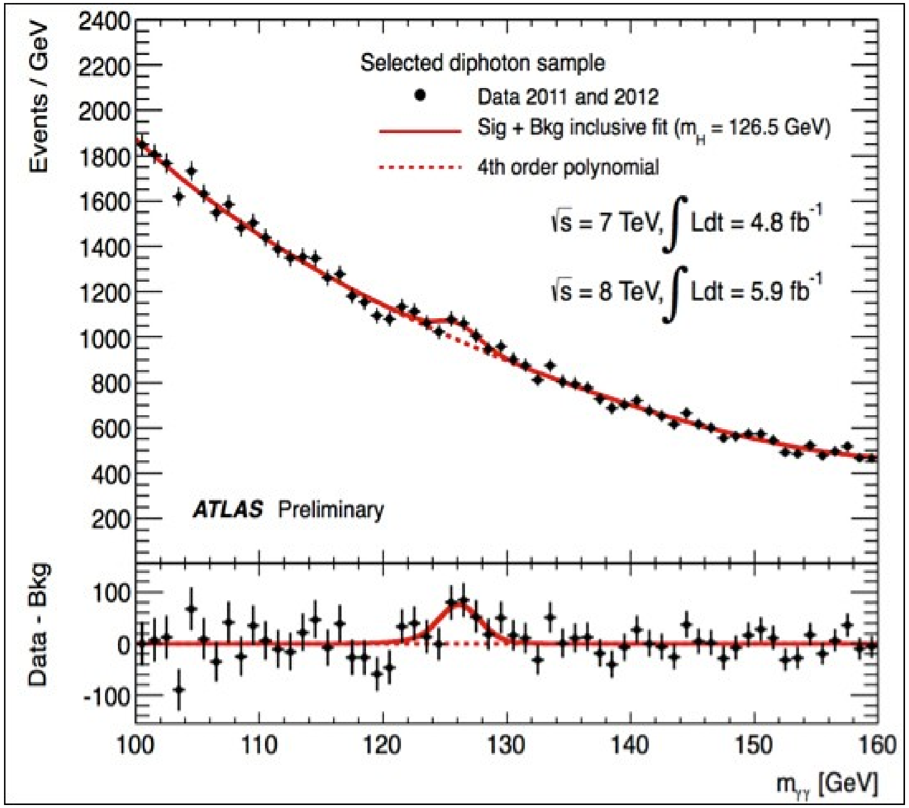

Peak width completely dominated by resolution effect (Γ_{SM} = 4 MeV)

$H \rightarrow \gamma\gamma + E_T^{miss}$: a performance driven channel

Missing energy reconstruction

- Missing transverse momentum :
  - Reconstructed using jet,e,γ,μ,τ + Soft-terms
  - Soft-terms : low energy clusters and/or tracks not associated to any object.

- Caveat : Pile-up → MET degradation.

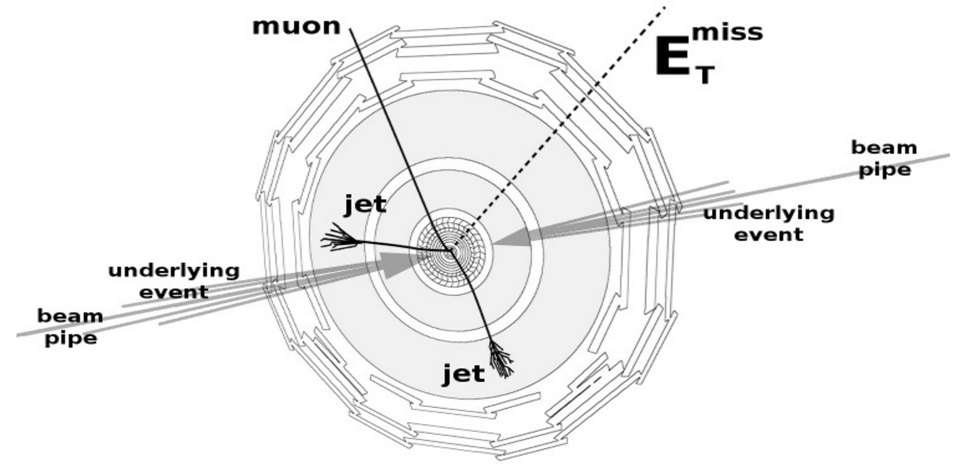

Soft-terms from clusters

Good energy

Bad vertex association

Bad pile-up rejection

Soft-terms from tracks

No neutral hadronic shower component

Good vertex association

Good pile-up rejection

Run II strategy

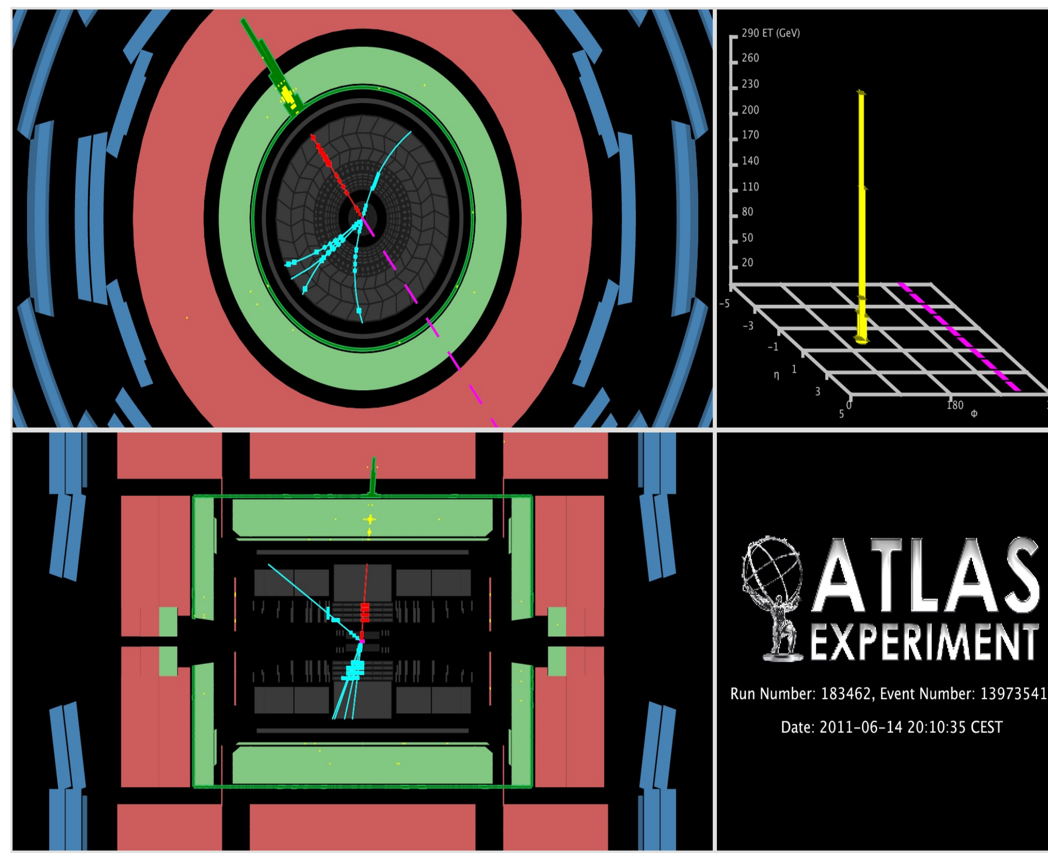

H → γγ + E_T^{miss} : a performance driven channel

Missing energy reconstruction

- Missing transverse momentum :
  - Reconstructed using jet,e,γ,μ,τ + Soft-terms
  - Soft-terms : low energy clusters and/or tracks not associated to any object.

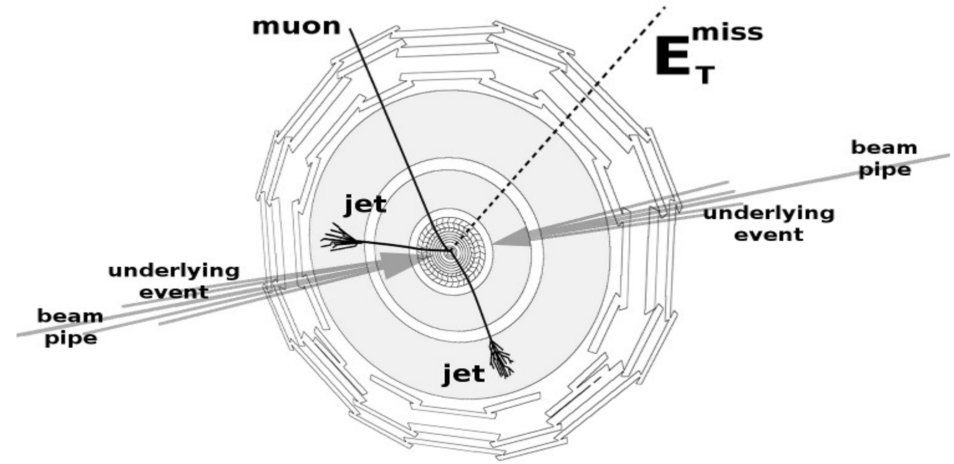

- Caveat : Pile-up → E_T^{miss} degradation.

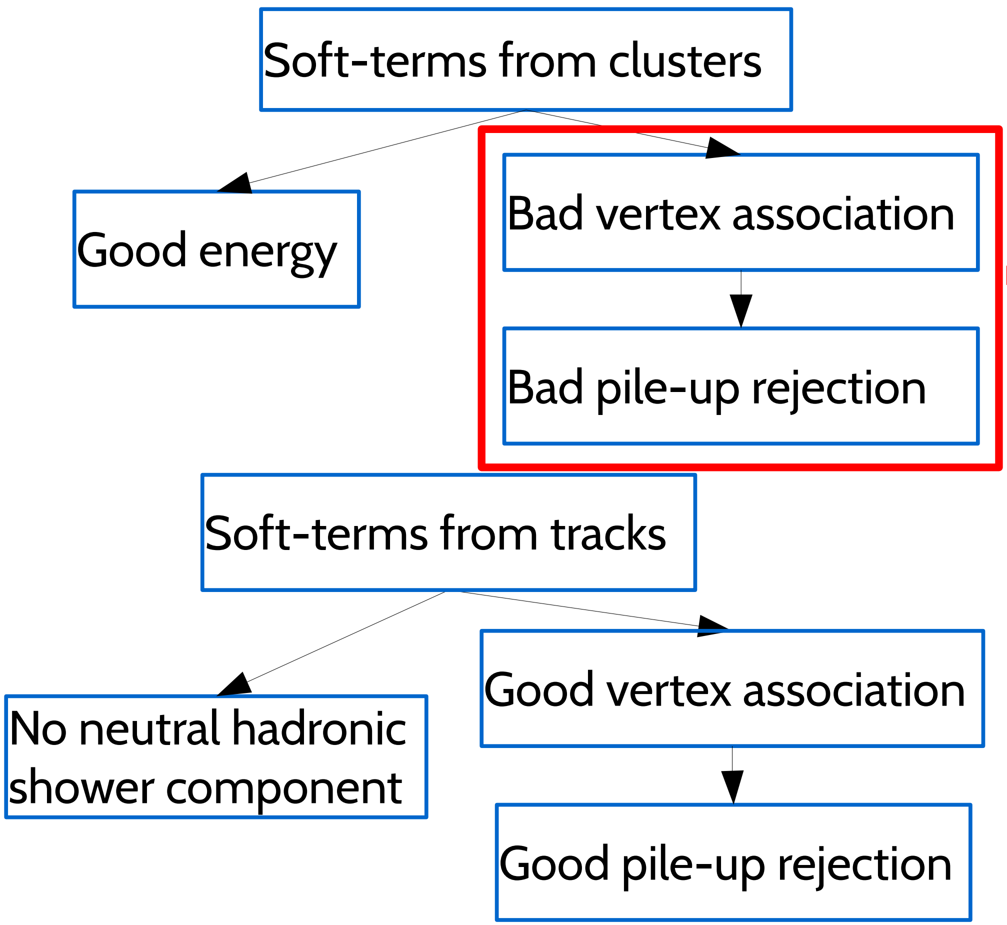

- If improvement in vertex association → Feasible to use clusters to calculate the soft-terms.
- Arrival time to detector → Use to estimate vertex

A part of my work was devoted to study performance of E_T^{miss} reconstruction.
Reduce timing resolution → Estimate vertex association improvement

Electromagnetic calorimeter

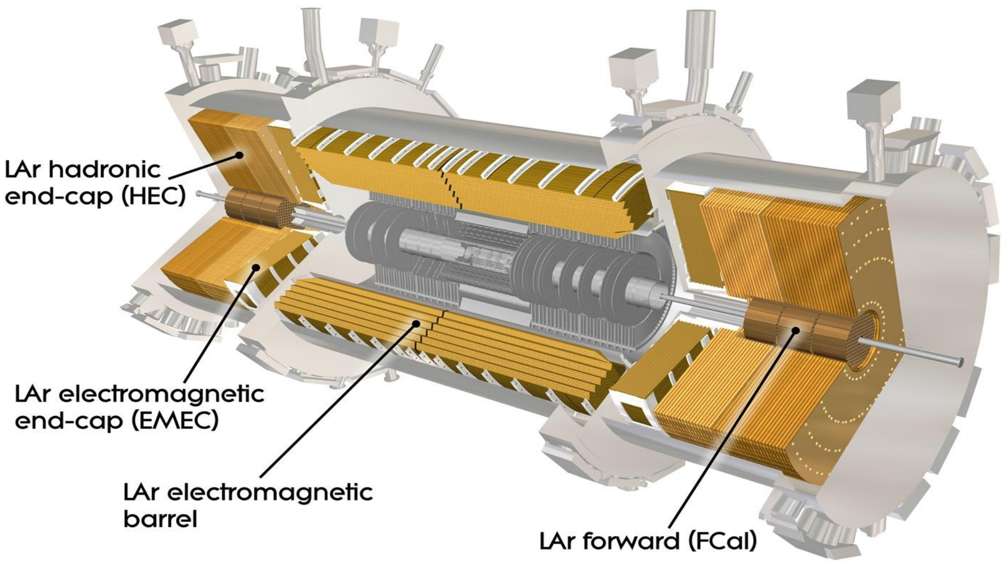

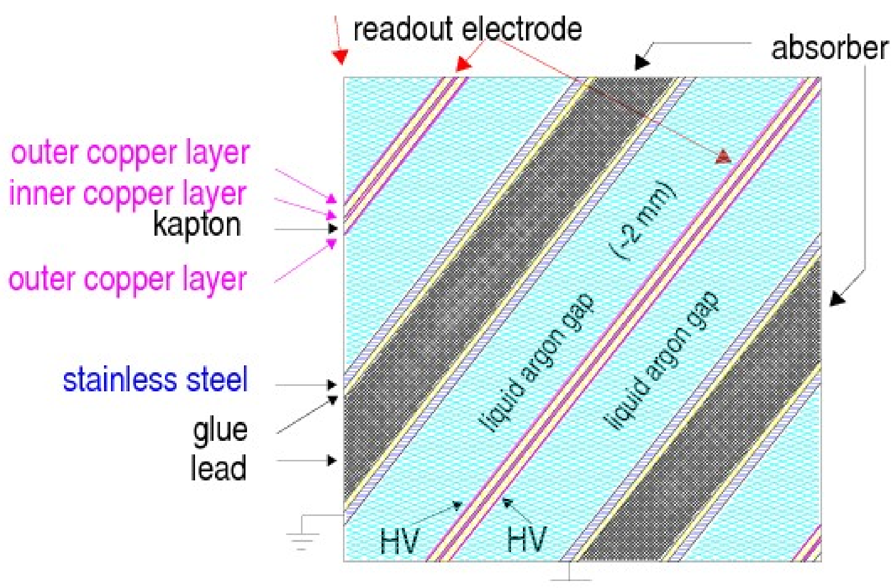

- Measure electromagnetic showers from e^- or γ and EM part of hadronic showers.
- LAr/Lead calorimeter
- Electrodes retrieve charges → Signal amplitude α Energy deposit
- Three sub-detectors:
  - One barrel ($|\eta| < 1.475$)
  - Two end-cap wheels ($1.375 < |\eta| < 3.2$)
  - Forward calorimeter ($3.2 < |\eta| < 4.9$)
- Segmented in three layers
  - First (highly segmented) → measure impact point.
  - Second → Measure main energy deposit
  - Third → Measure energy and leakage

Electromagnetic calorimeter

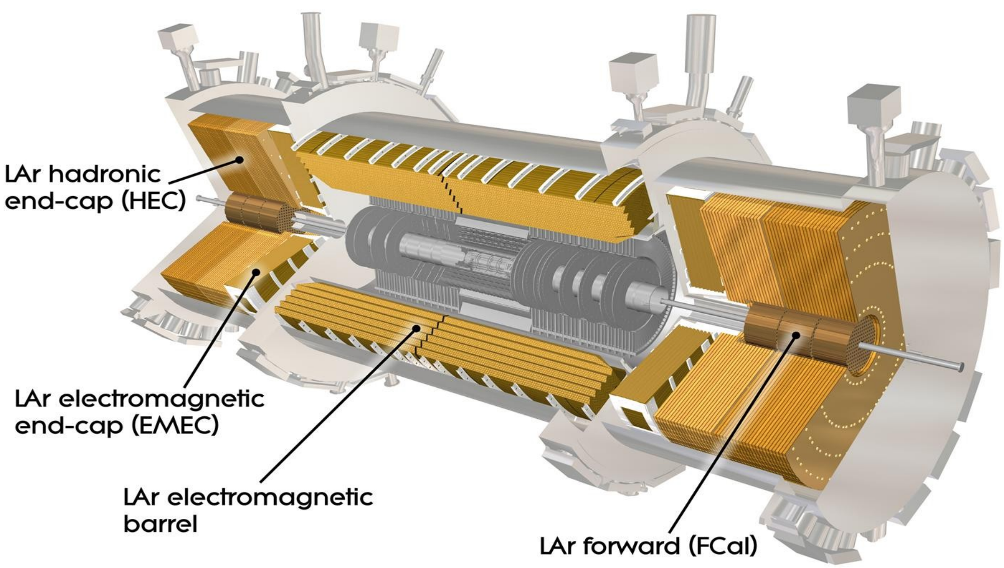

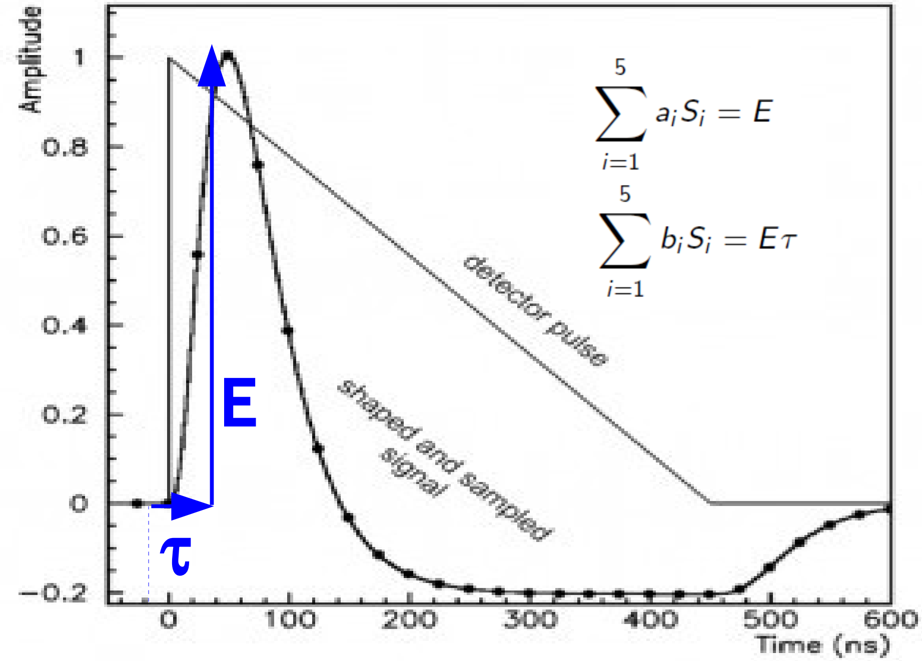

$$E_{cell} = F_{\mu A \to MeV} F_{DAC \to \mu A} \frac{1}{\frac{M_{phys}}{M_{calib}}} \sum_{j=0}^{2} R_j \left(\sum_{i=0}^{4} a_i S_i \right)$$

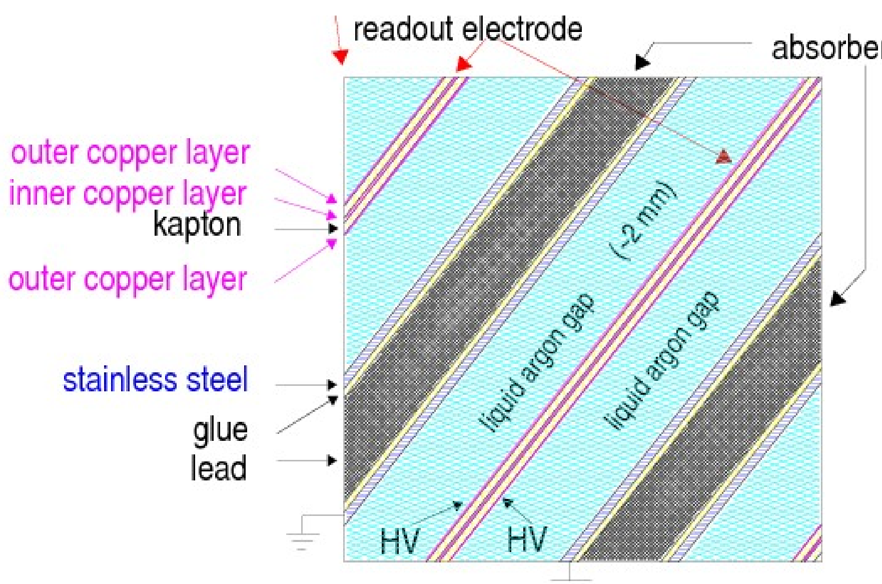

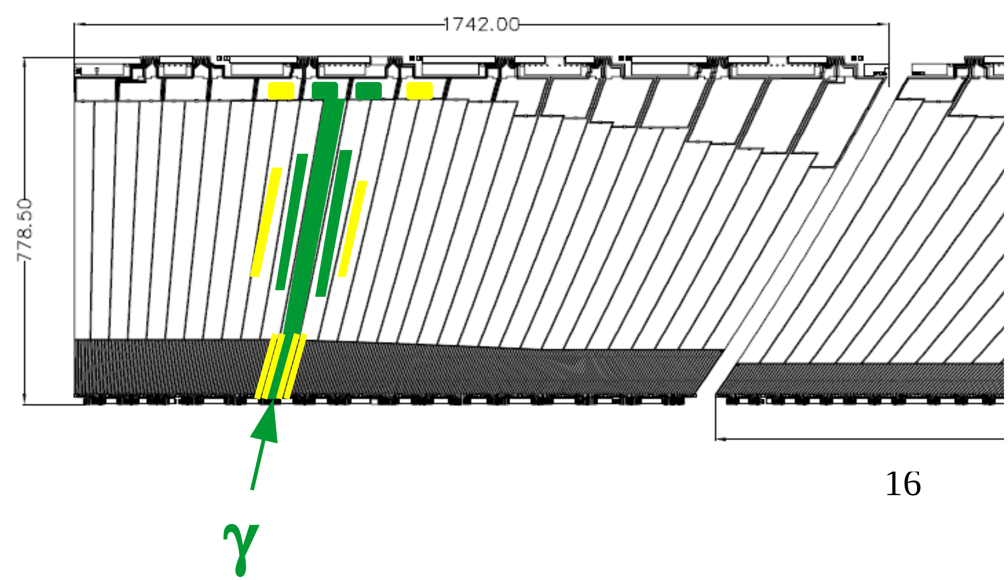

Electromagnetic calorimeter

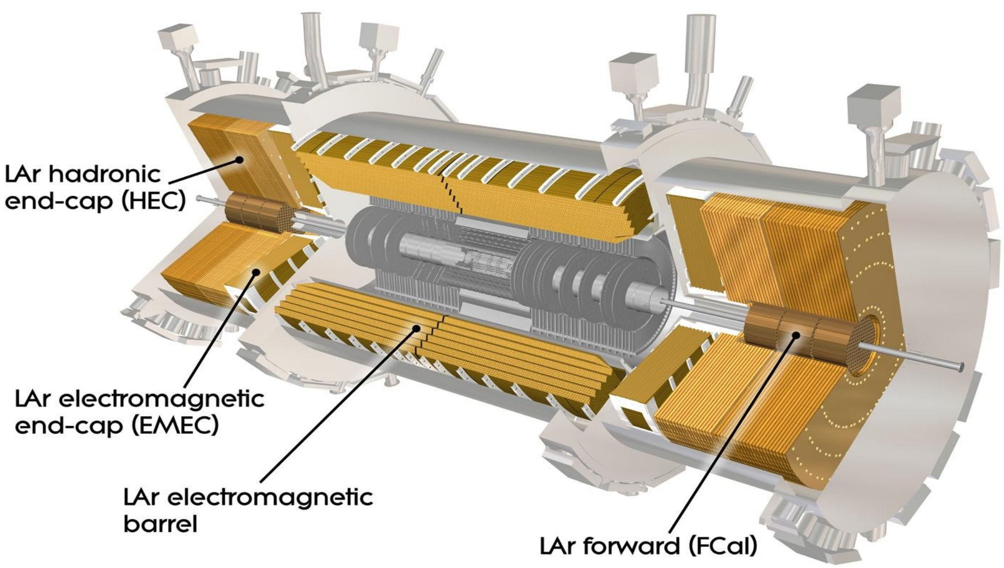

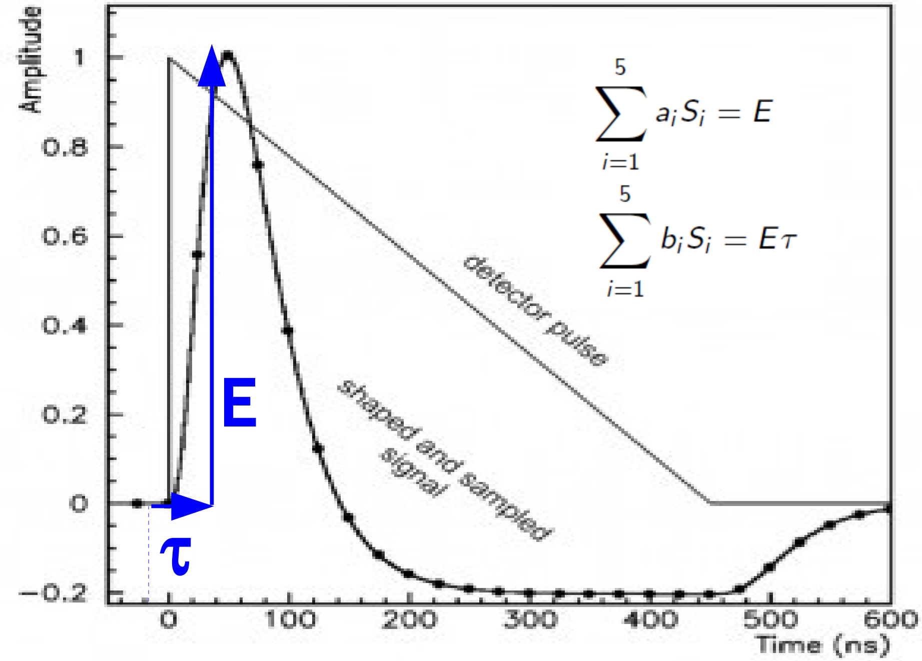

$$E_{cell} = F_{\mu A \to MeV} F_{DAC \to \mu A} \frac{1}{\frac{M_{phys}}{M_{calib}}} \sum_{j=0}^{2} R_j \left(\sum_{i=0}^{4} a_i S_i \right)$$

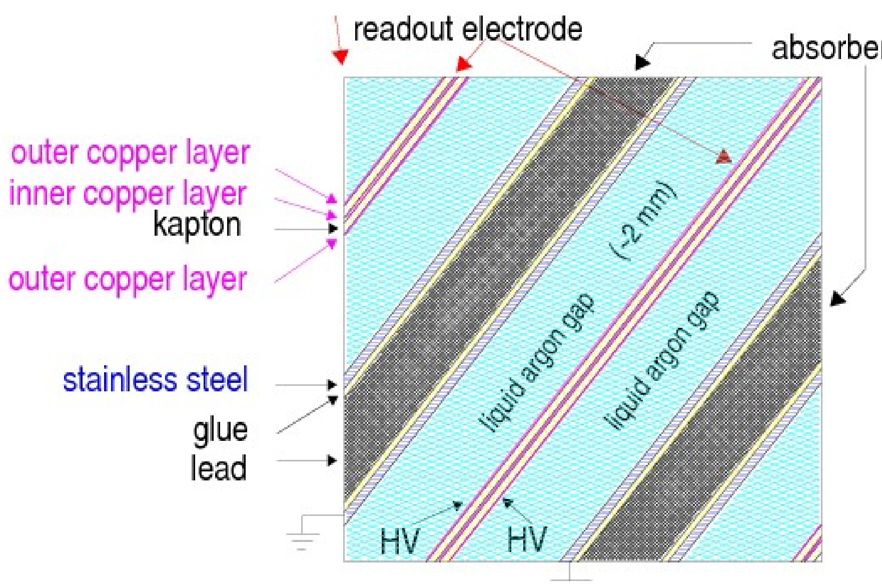

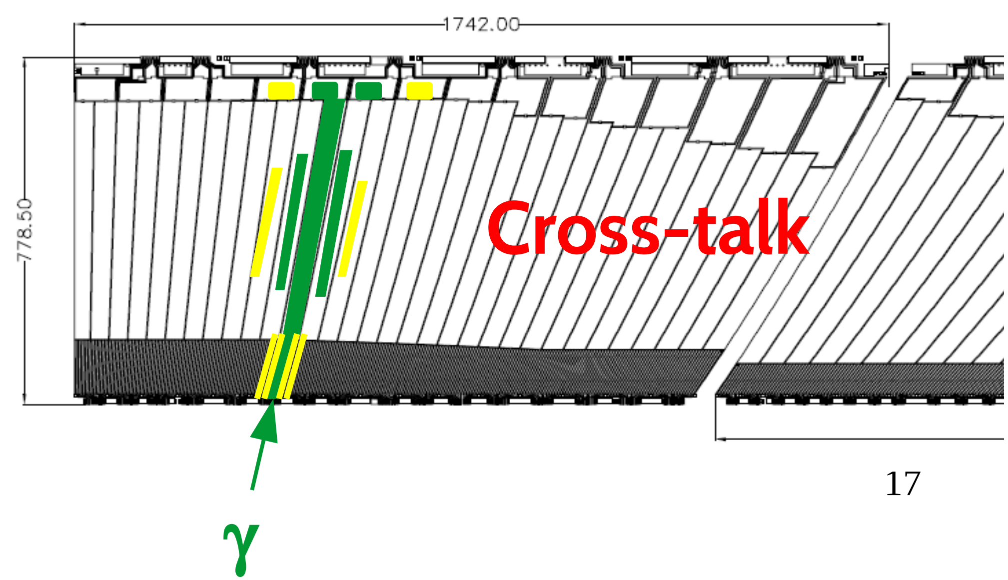

Improvement in performance : Cross-talk in EM barrel

- Charge transfer between cells.
- Couplings in the detector : close cells or readout chain.

- **Cross-talk introduces distortion to signal shapes.**
  - Increases energy and time uncertainty for that cell.

- **Cross-talk also distorts shower shapes**
  - Introduces sizeable signal in cells receiving no energy from the EM shower.

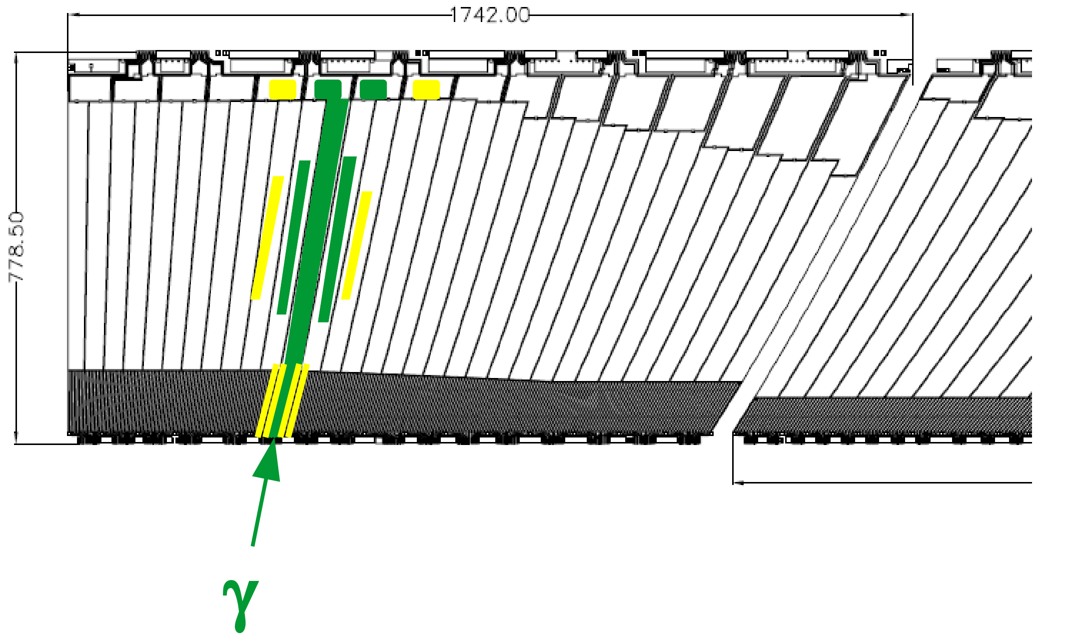

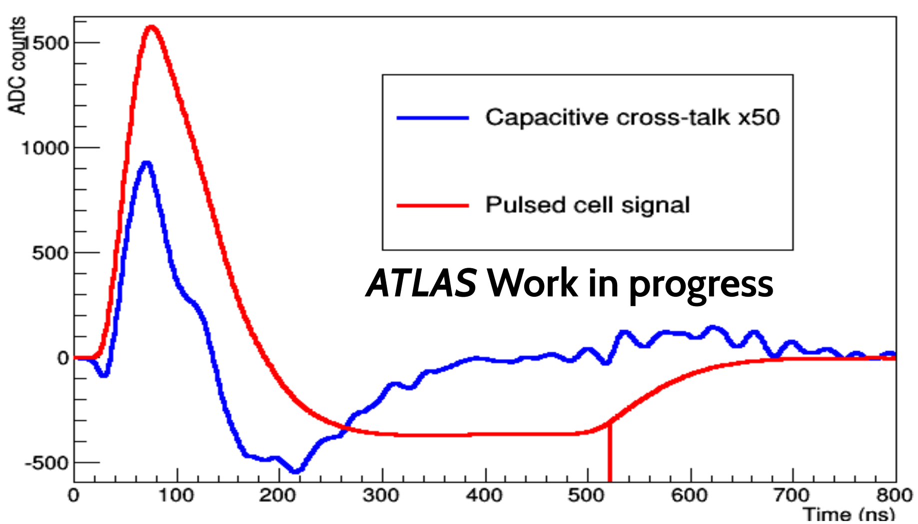

- According to previous studies , effect of cross-talk in the **time resolution of the LAr Barrel is around 94 ps.**

- At c, 100 ps = 3 cm in the vertex identification
- Interaction point spread has a σ ~ 6 cm.

- Reducing cross-talk → **Improve time resolution (150 ps → 50 ps for 60 GeV e^- if all cells in a cluster are taken into account)**

Types of cross-talk in EM barrel

- **Capacitive :**
  - High segmentation provokes couplings between cells.
  - Higher when segmentations is finer.

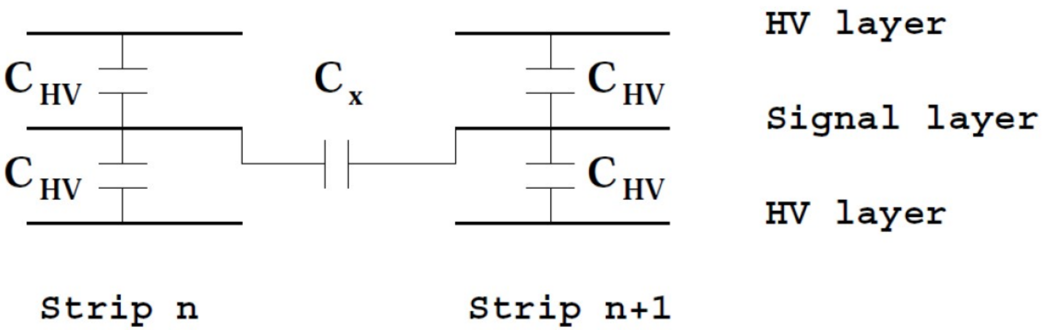

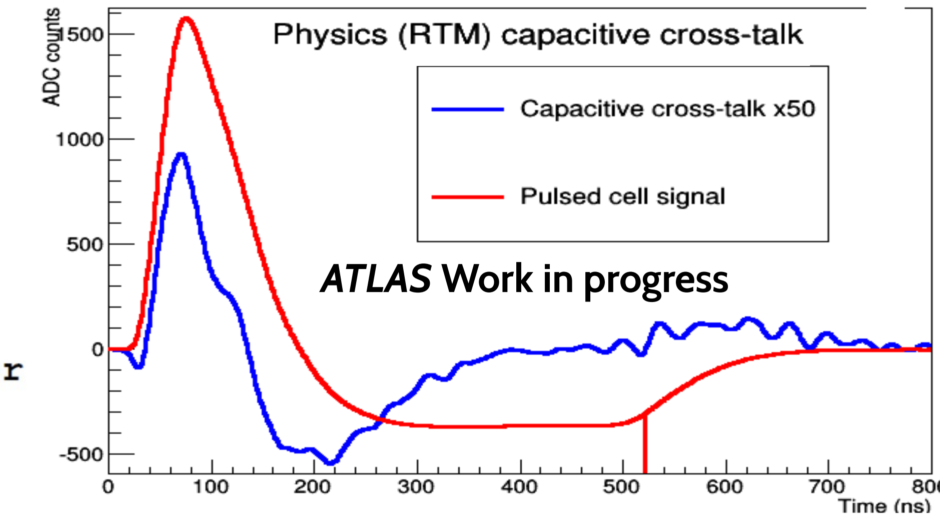

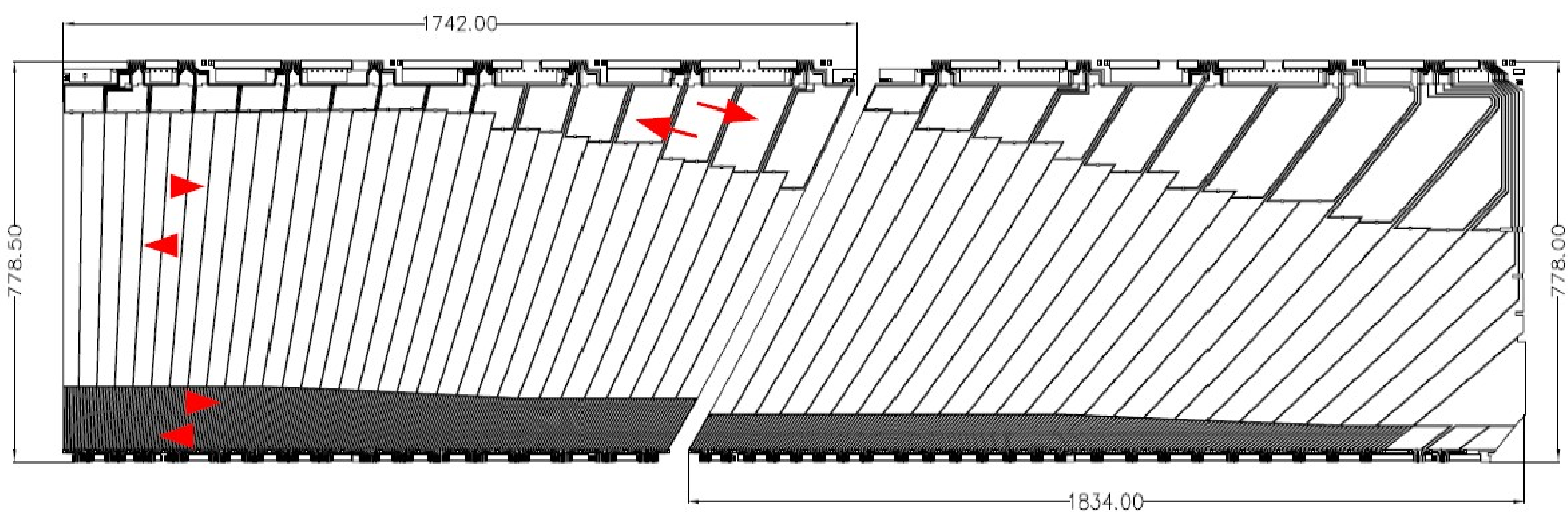

Types of cross-talk in EM barrel

- **Resistive**
  - HV layer providing calorimeter with high readout voltage is presents serigraphed resistors between the first and second layer.

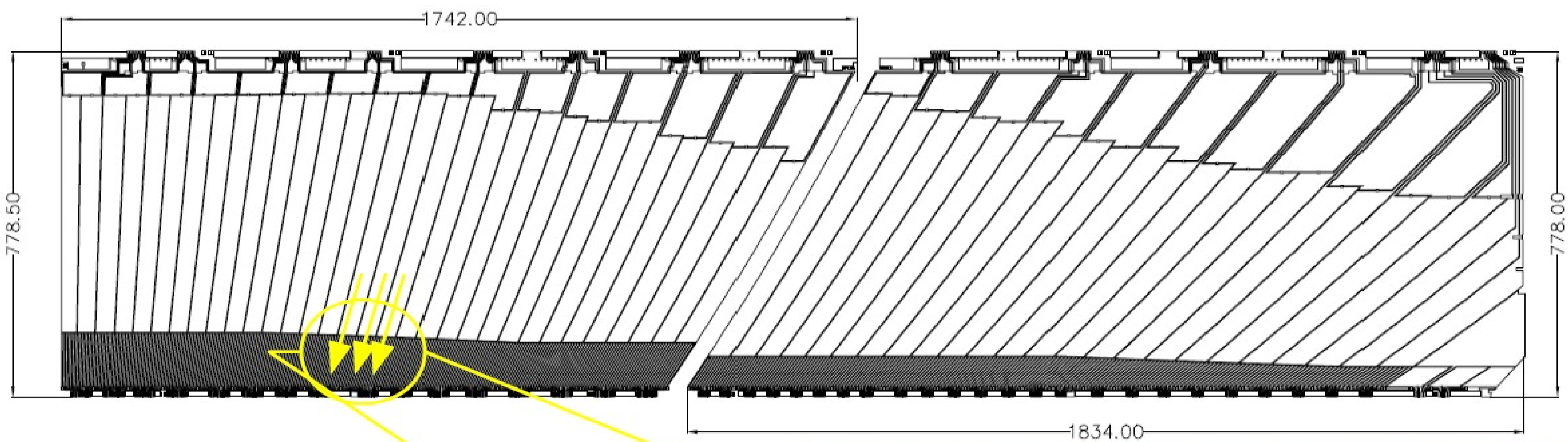

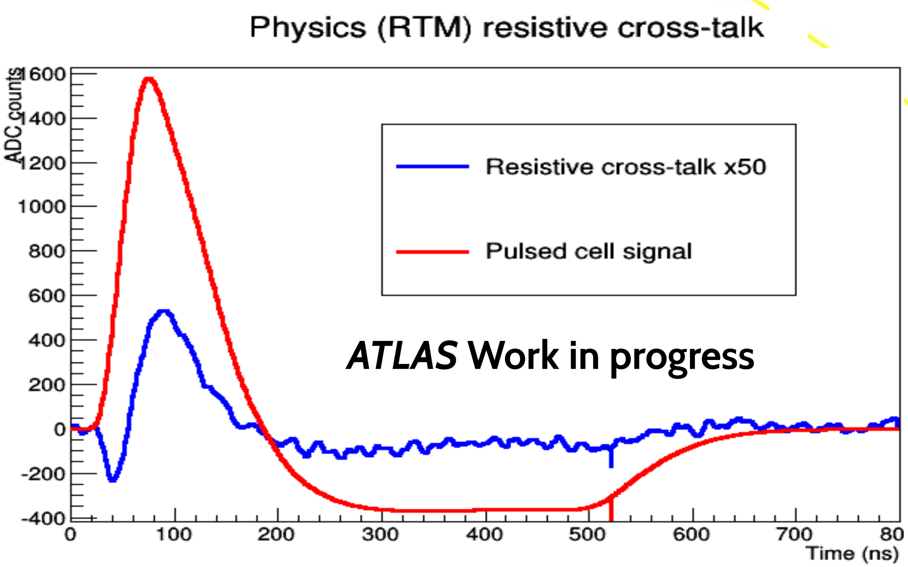

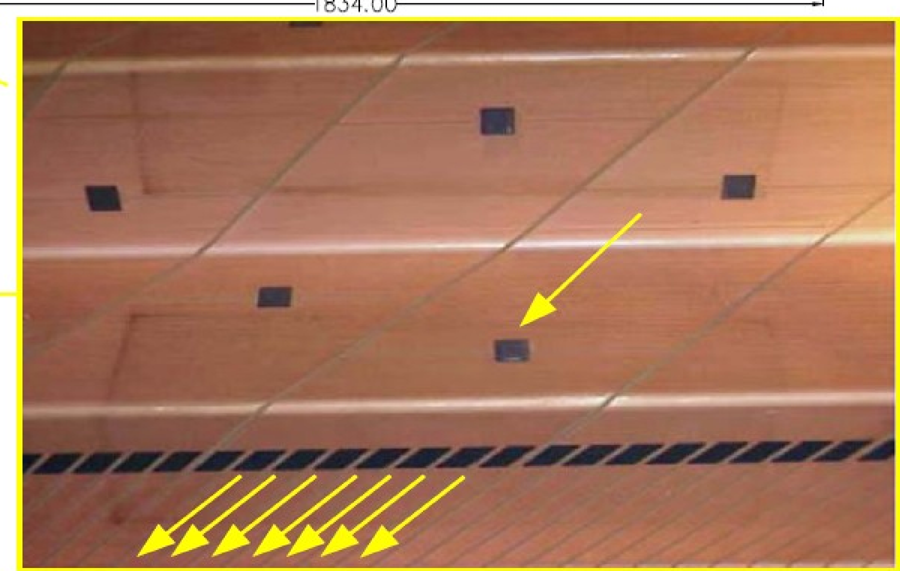

Types of cross-talk in EM barrel

- **Inductive:**
  - Readout cables are connected to mother boards very closely.
  - When current is passing in one cable, a charge is inducted in the others.

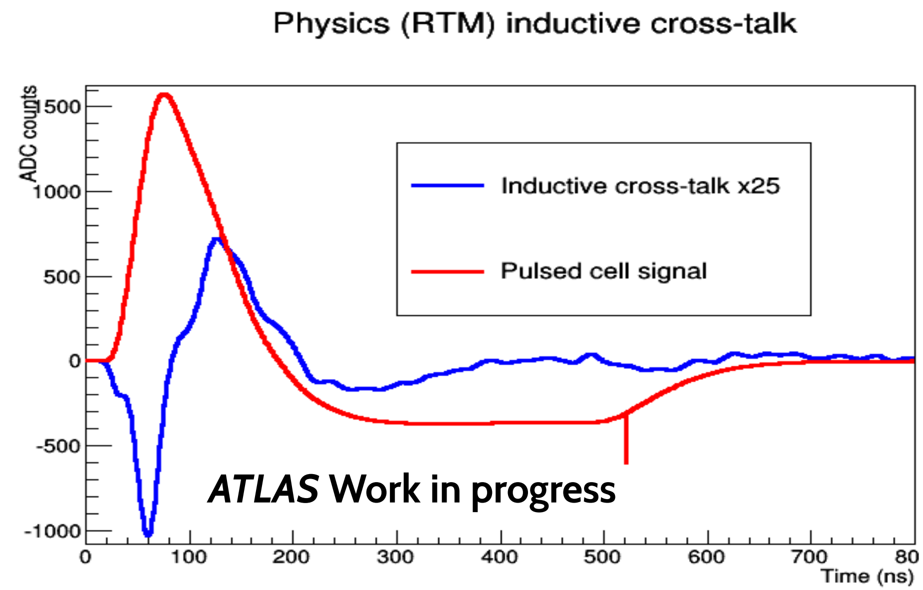

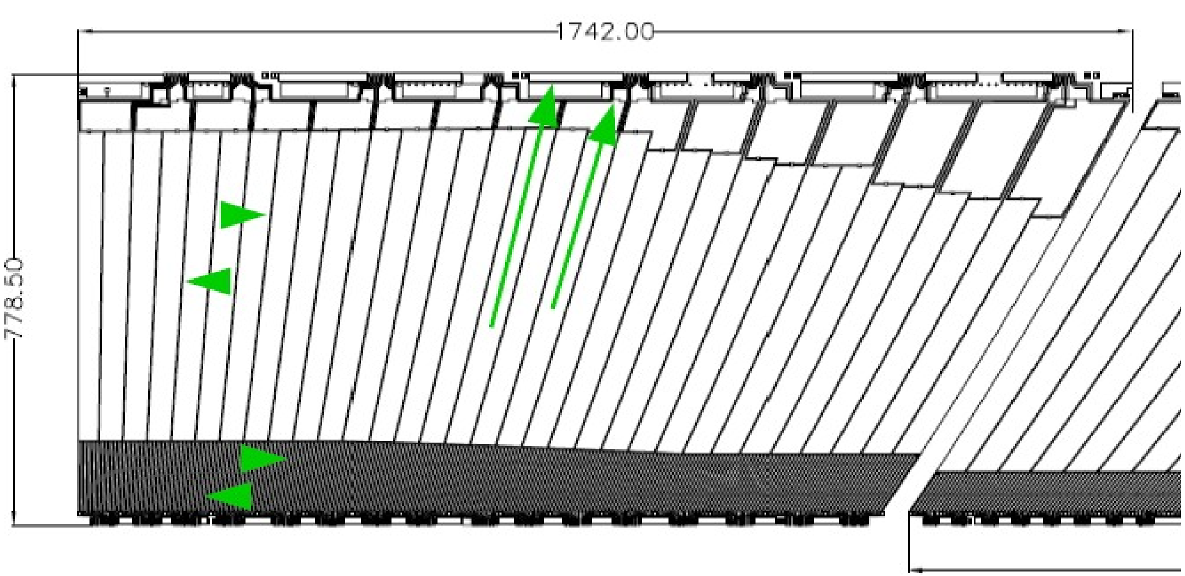

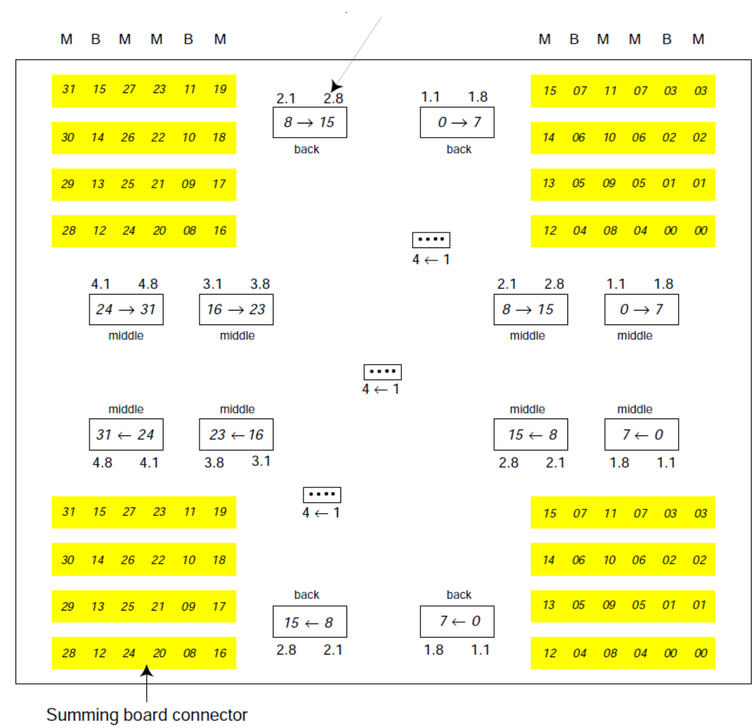

Types of cross-talk in EM barrel

- **Inductive:**
  - Readout cables are connected to mother boards very closely.
  - When current is passing in one cable, a charge is inducted in the others.
  - Long distance :
    - Due to coupling in the cryostat feedthroughs.
    - Charge transfer between cells in different regions of the calorimeter.

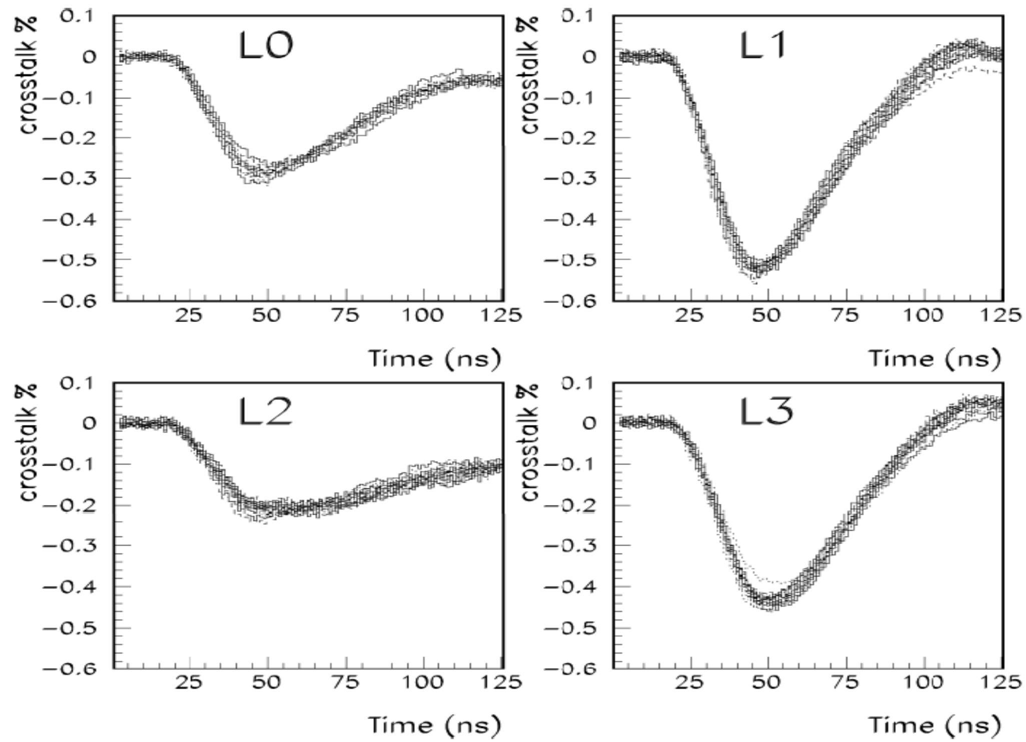

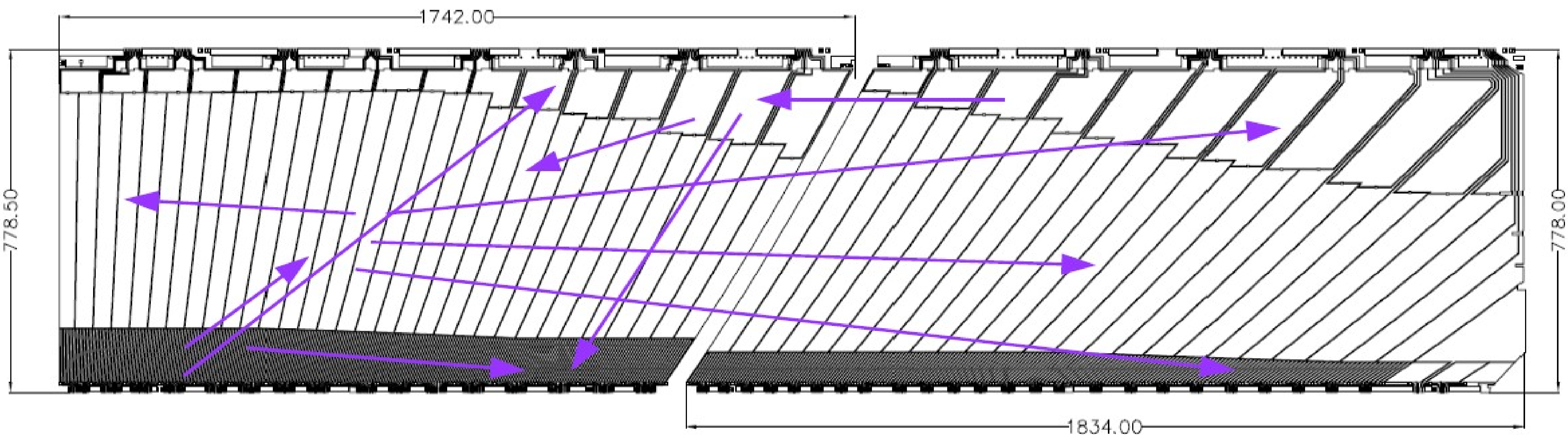

Cross-talk studies from ATLAS commissioning

- Studied using calibration signals (different shape than from physics pulses).
  - **Studied peak-to-peak and under peak-to-peak ratios.**
- Calibration signals shape is different from physics signal.
- No energy nor sample-by-sample cross-talk estimation
- **My qualification work was to study this cross-talk in detail and to measure its real impact on energy measurement in the LAr Barrel.**

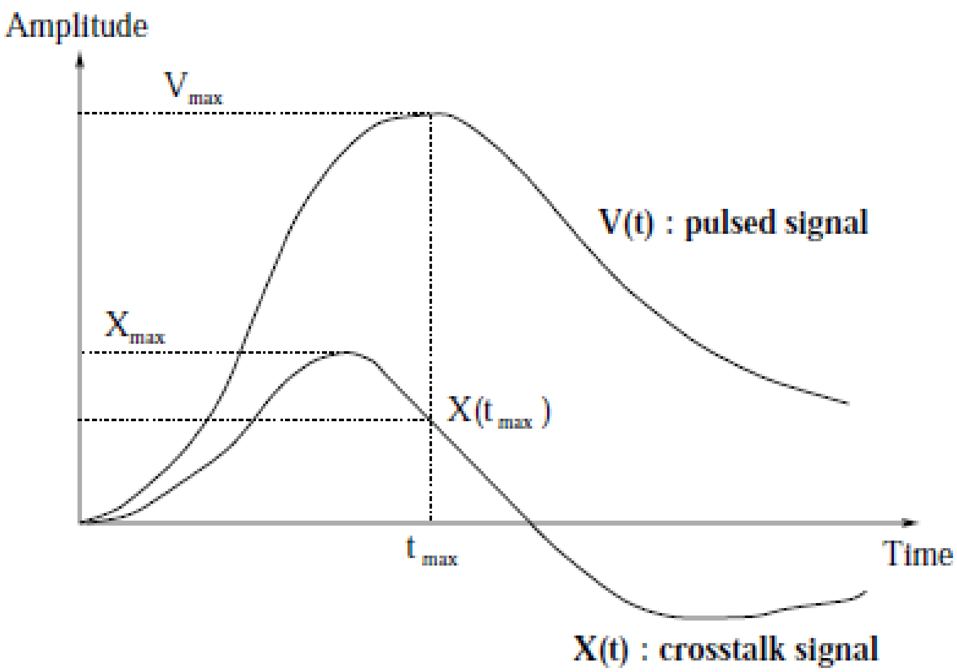

Mean cross-talk values	Type	Peak-to-peak	Under peak-to-peak
Layer 1 → 1	Capacitive	7.15 %	4.5%
Layer 2 → 1	Resistive	0.089%-0.099%	0.070%-0.093%
Layer 2 → 2	Inductive	1.11 %	0.44%
Layer 2 → 3	Inductive	0.88%	0.61%
Layer 3 → 3	Inductive	1.43%	-0.52%

Cross-talk studies

- Cross-talk is studied with **special calibration runs.**
- Calibration signal → Physics signal
  - **Calibration injects decreasing exponential pulse** → **Physics pulse is a triangle.**

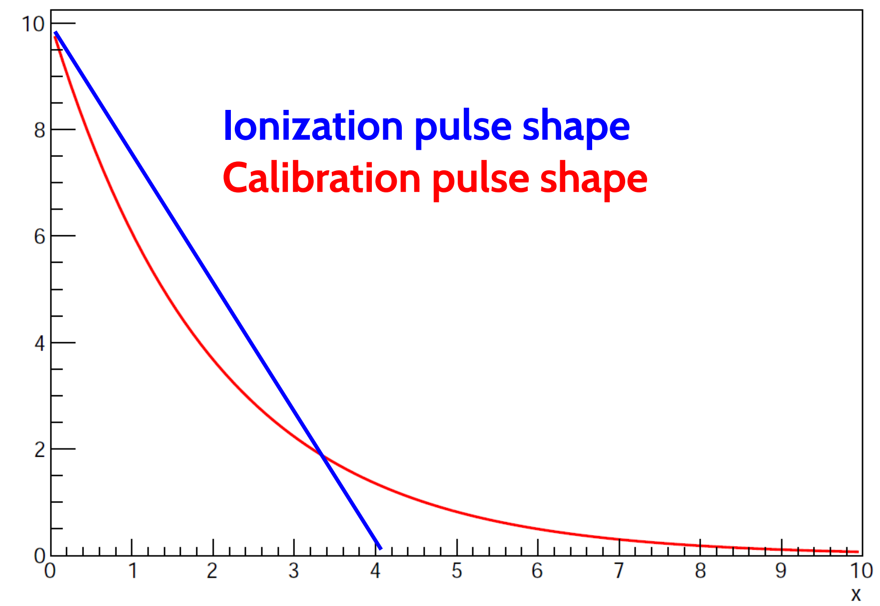

Cross-talk studies

- Cross-talk is studied with **special calibration runs.**
- Calibration signal → Physics signal
  - Calibration injects decreasing exponential pulse → Physics signal is a triangle.
  - Physics signal produced by particles entering the front part of detector.

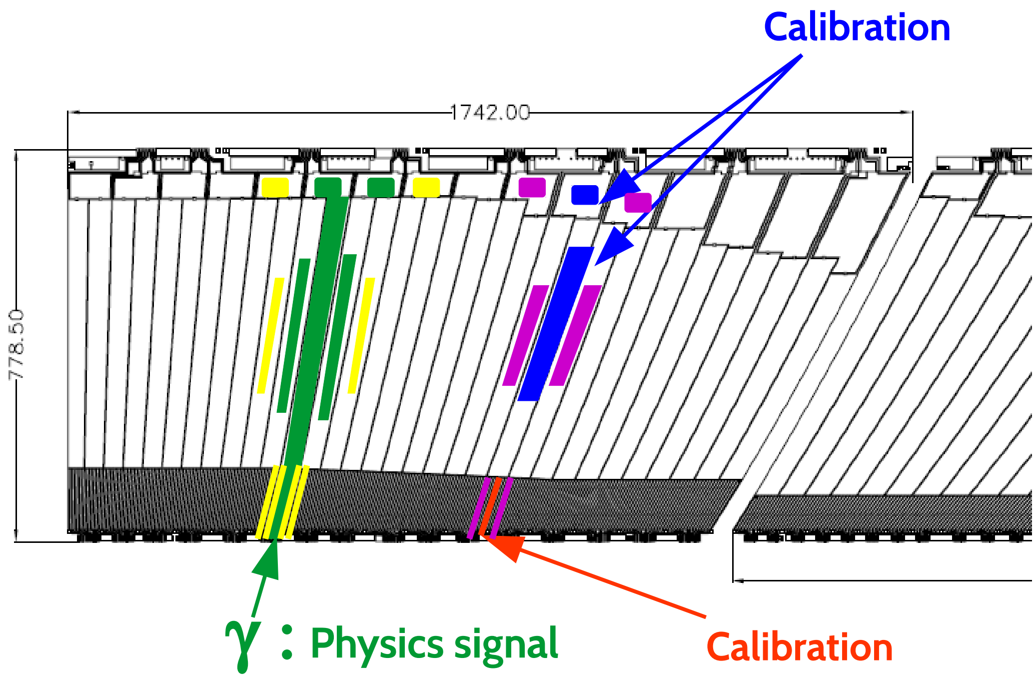

Cross-talk studies

- Cross-talk is studied with **special calibration runs.**
- Calibration signal → Physics signal
  - Calibration injects decreasing exponential pulse → Physics signal is a triangle.
  - Physics signal produced by particles entering the front part of detector.
- Physics signal extraction can be done with several methods → Introduce response functions.
  - Use the nominal one (RTM)

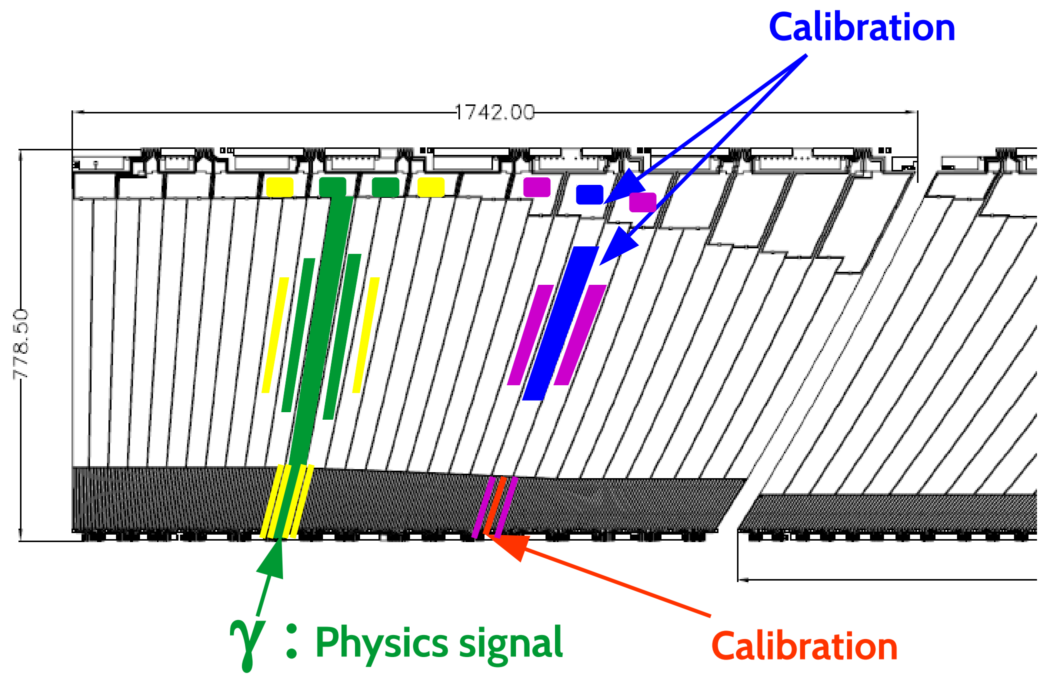

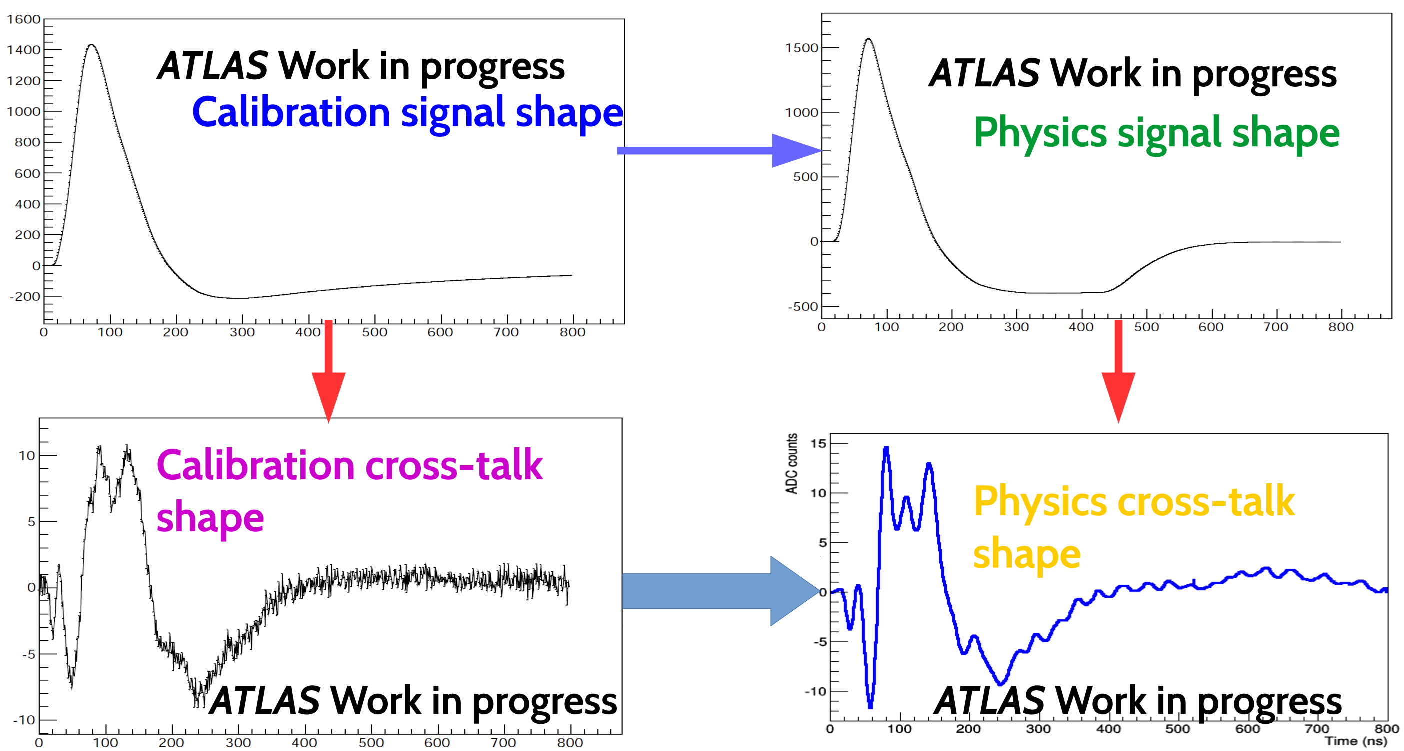

Cross-talk studies

- Cross-talk is studied with **special calibration runs.**
- Calibration signal → Physics signal
  - Calibration injects decreasing exponential pulse → Physics signal is a triangle.
  - Physics signal produced by particles entering the front part of detector.
- Physics signal extraction can be done with several methods → Introduce response functions.
  - Use the nominal one (RTM)
  - **Matrix method → Used for systematics**

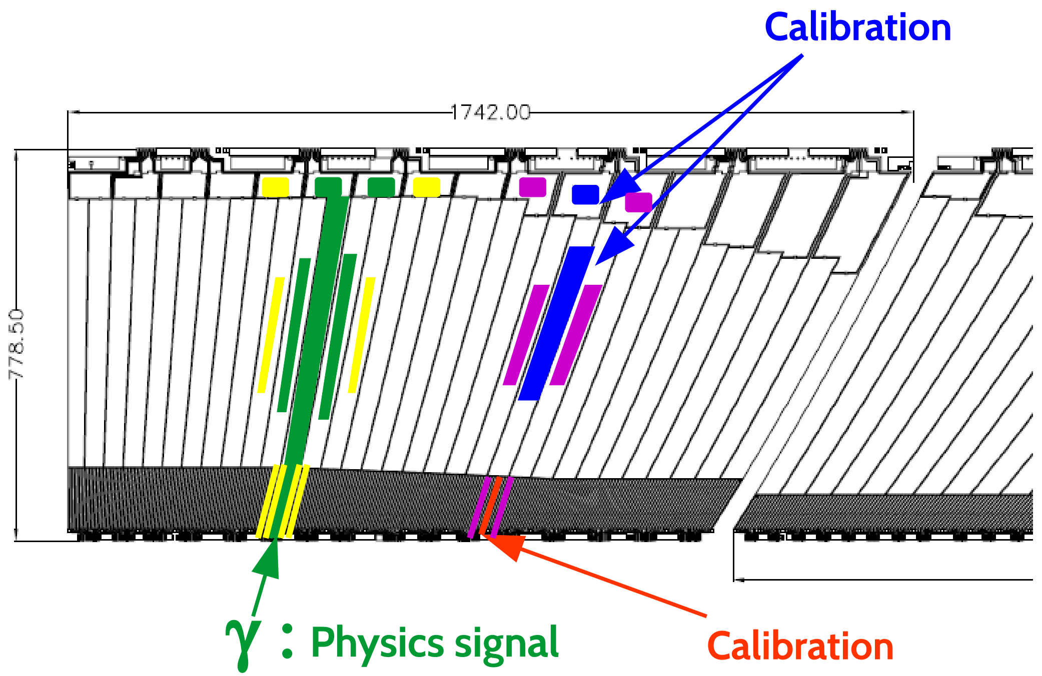

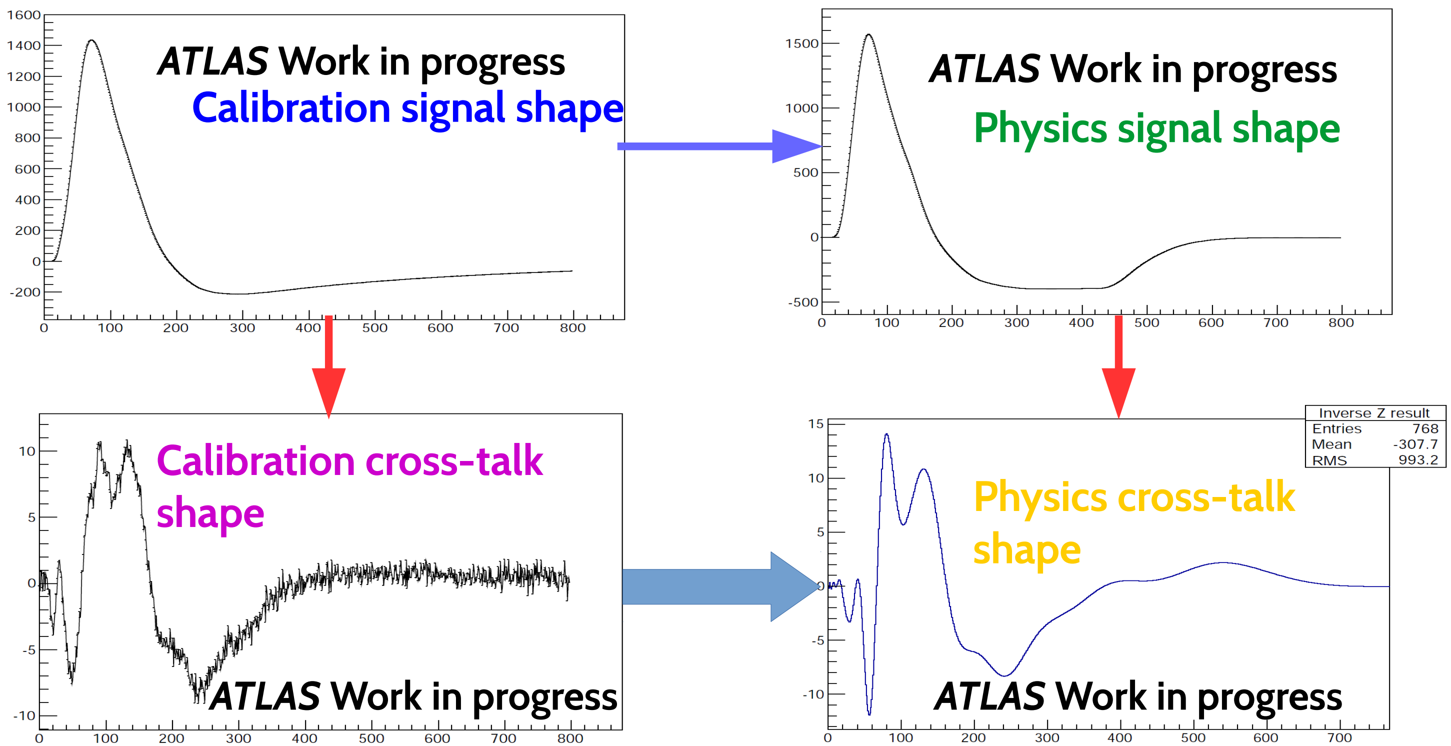

Physics cross-talk reconstruction methods

RTM method

- Time domain
- Convolution

$$g^{XTalk}_{Phys} = g^{XTalk}_{Calib} \; * \; H(t)_{exp\to tri} \; * \; H(t)_{MB\to det}$$

χ^2 method

- Same as matrix → $S(t_n)$ taken from χ^2 minimisation

$$\chi^2 = \sum_{i=0}^{M} \left| \frac{\left(\sum_{n=0}^{N-1} a_n z_i^{-n} - \frac{S_{phys}(z_i) S^{XTalk}_{calib}(z_i)}{S_{calib}(z_i)} \right)^2}{\sigma^2} \right|$$

Matrix method

- Time domain → Discrete Laplace domain (Z transform). $\zeta(a[n]) = \sum_{n=0}^{N-1} a_n z^{-n}$
- Multiply response functions
- Apply inverse Z transform
  - Matrix inversion.

$$S(z)^{XTalk}_{Phys} = \frac{S(z)^{XTalk}_{Calib} S(z)_{Phys}}{S(z)_{Calib}} \qquad S(z)^{XTalk}_{phys} = \sum_{n=0}^{N-1} S(t_n)^{XTalk}_{Phys} z^{-n}$$

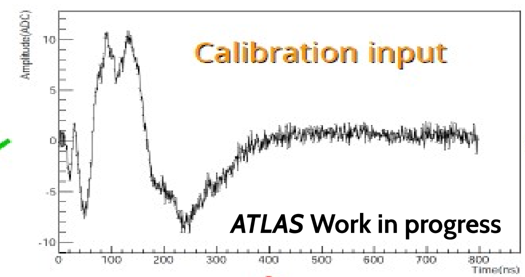

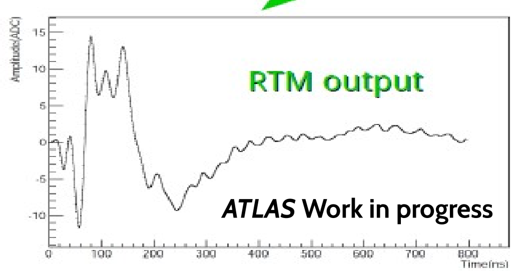

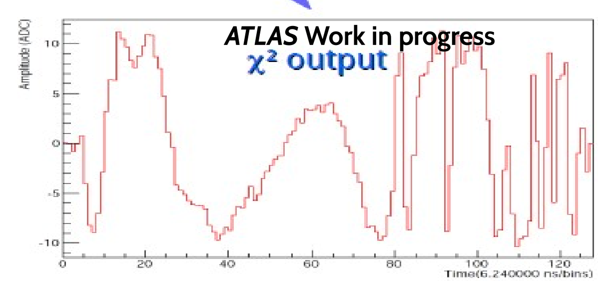

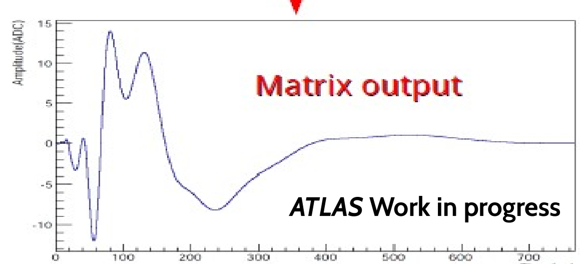

Energy and time extraction at cluster level

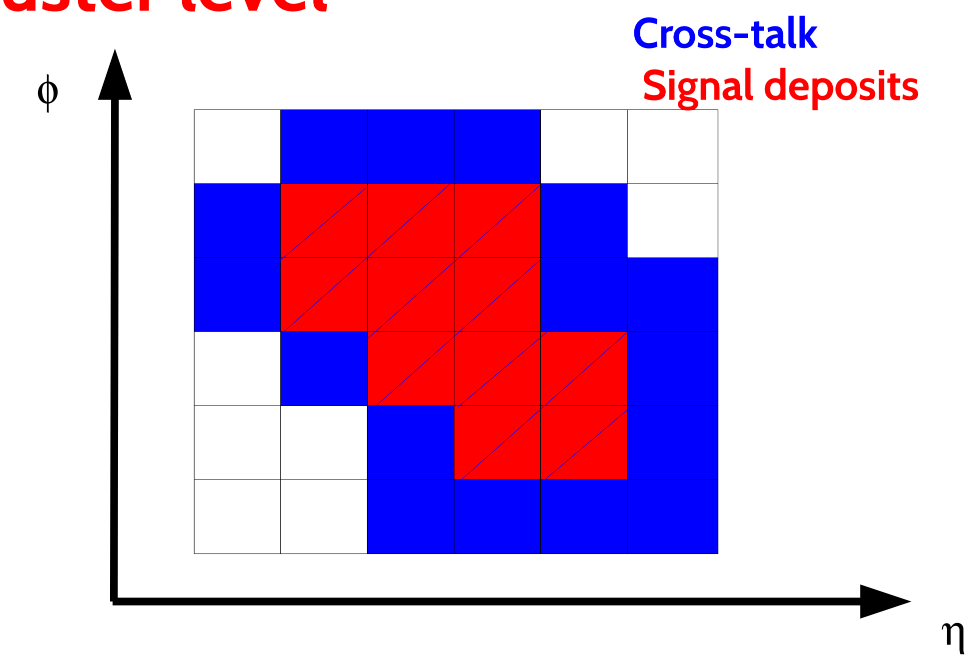

Correct cross-talk

- Signal in one cell = True ionization signal + cross-talk from surrounding cells:

$$S_i^k = \sum_j X_{i\leftarrow j}^k S_j^{k,True}$$

Measured quantities

$$X = \begin{pmatrix} 1 & X_{1\leftarrow 2} & \cdots & X_{1\leftarrow n} \\ X_{2\leftarrow 1} & 1 & \cdots & X_{2\leftarrow n} \\ \vdots & \vdots & \ddots & \vdots \\ X_{m\leftarrow 1} & X_{m\leftarrow 2} & \cdots & 1 \end{pmatrix}$$

- At the same time, signal is :

$$S_j^{k,True} = E_j^{True} g(t_j^k, \tau_j^{True}) + n_j^k$$

Energy deposit without cross-talk

Modeled signal τ without cross-talk

Cell noise

$$E_i = \sum_k a_i^k S_i^k = \sum_k a_i^k \sum_j X_{i\leftarrow j}^k (E_j^{True} g(t^k, \tau_j^{True}) + n_j^k)$$

$$E_i \tau_i = \sum_k b_i^k S_i^k = \sum_k b_i^k \sum_j X_{i\leftarrow j}^k (E_j^{True} g(t^k, \tau_j^{True}) + n_j^k)$$

E_j^{True}, τ_j^{True} and noise term can be retrieved optimally for each cell in a cluster

Expected performance improvement from cross-talk corrections

Signal shape distortion after cross-talk correction:

- Signal shape is known. Pile-up affected cells could then be identified by bad quality fits and corrected.

Energy improvement :

- Cross-talk is not well simulated in Run I. Cross-talk correction can improve data/MC agreement → reduce systematics.

Time improvement

- Calorimetric cluster vertex association allows charged + neutral contributions tagging.
- Could open the option to use all cluster cells to extract a cluster time stamp → Reduce in-time and out-of-time pile-up.

Shower shapes distortion improvement

- Improve E1/E2 ratio → One of the main systematics in calibration.
- Improved MVA calibration.
- Better data/MC agreement → Reduce corrections applied to MC.

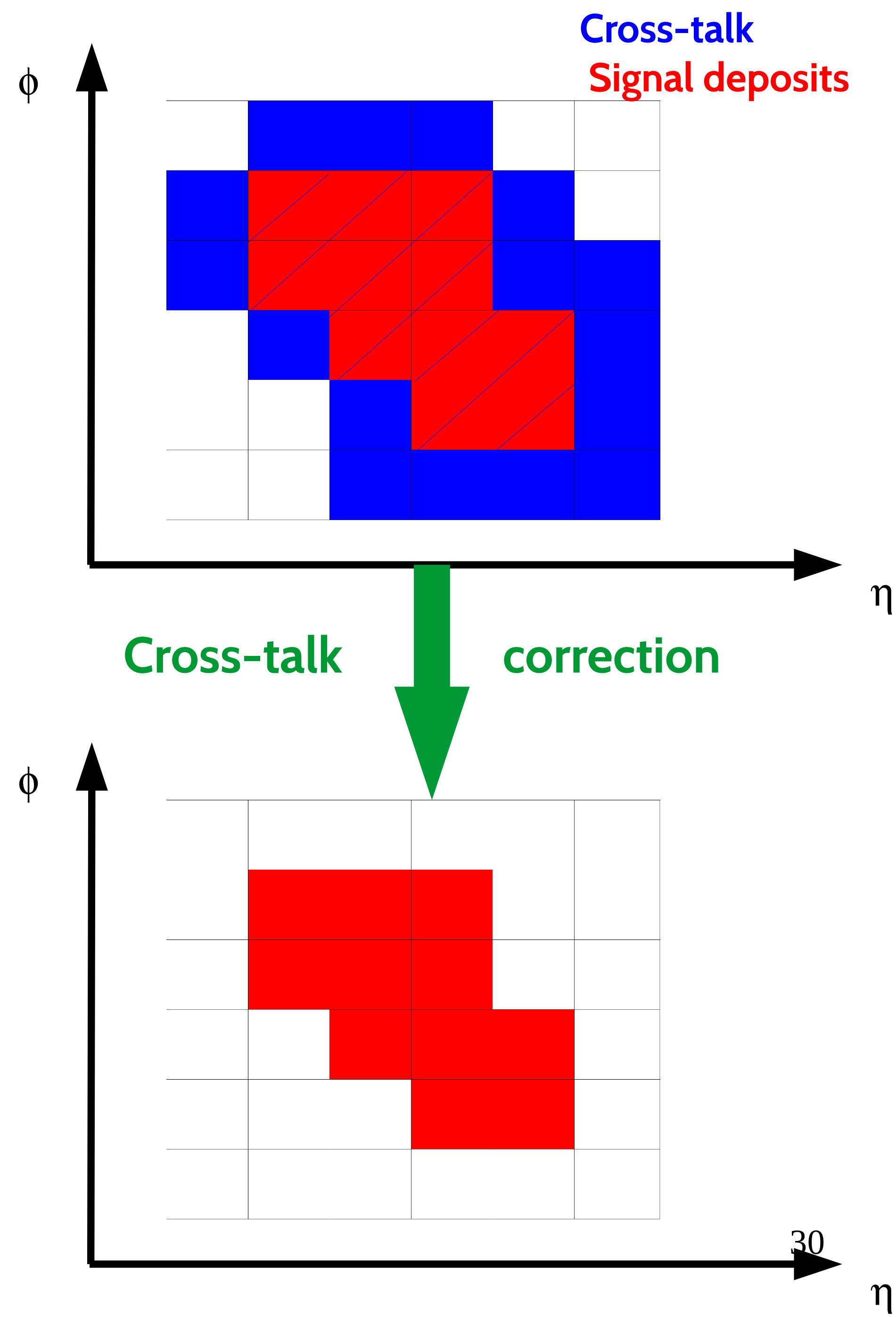

Conclusion

- Run I analysis sees an excess of 1.4 σ→ Interpreted as limits on couplings and EFT operators.
- **H → γγ + MET channel is driven by performances**.
- LAr detector presents cross-talk.
  - Studied its contribution for physics and energy.
- Cross-talk corrections expected to improve shower shape description and pile-up rejection → **Improve in H → γγ + MET measurements**
  - Better photon reconstruction and ID
  - CST MET less affected by pile-up.

Back-up

The ATLAS detector

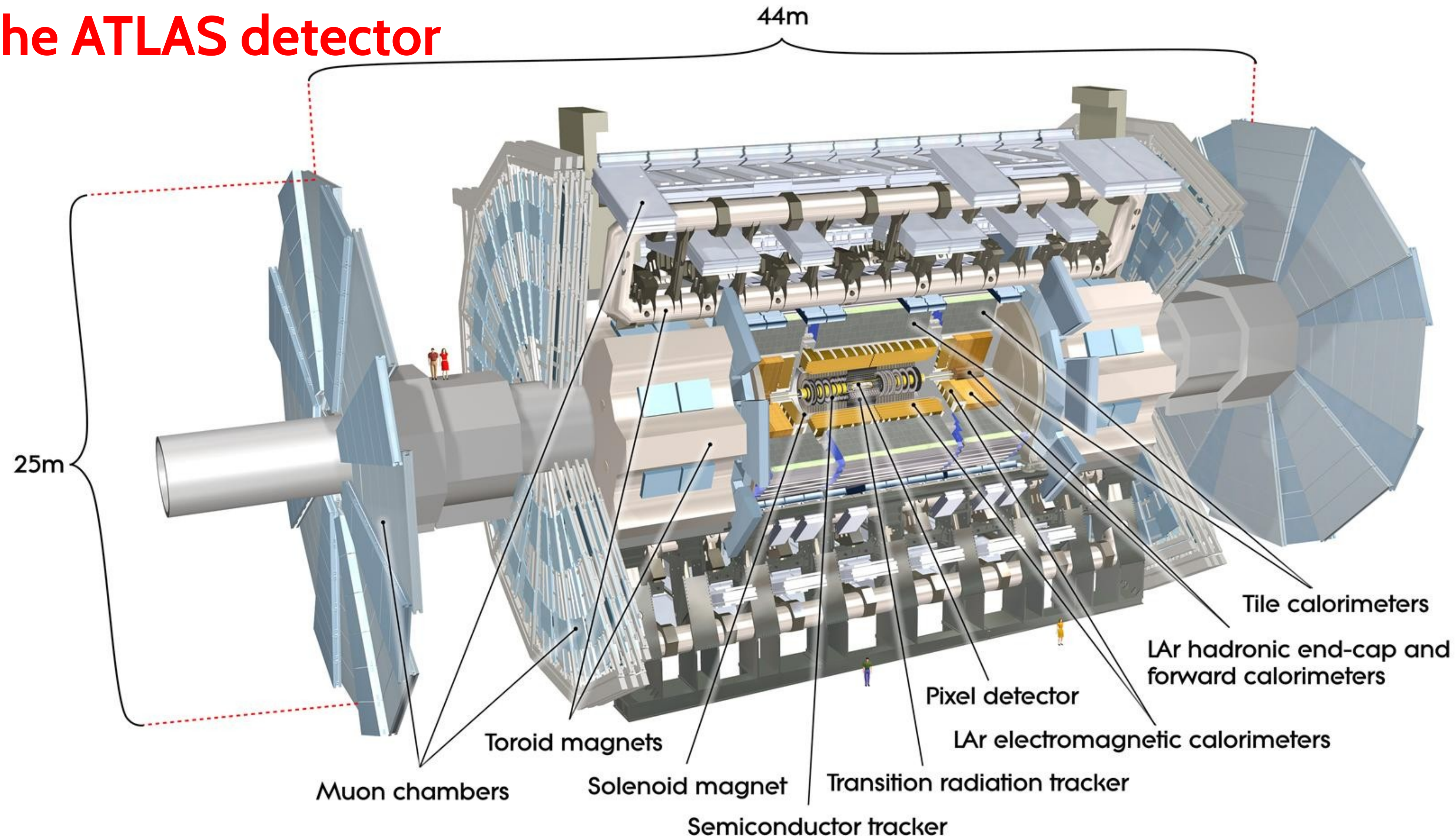

- Proton-proton collisions take place in the center of the detector.
  - Beams collimated so that little transverse displacement is achieved.
  - Every 25 ns.

- Pile-up :
  - High collision rate → High probability that disjoint interactions affect each other.
  - Energy and time measurements affected.
  - Lowered performance.

ATLAS Tracker and Calorimeter energy resolution

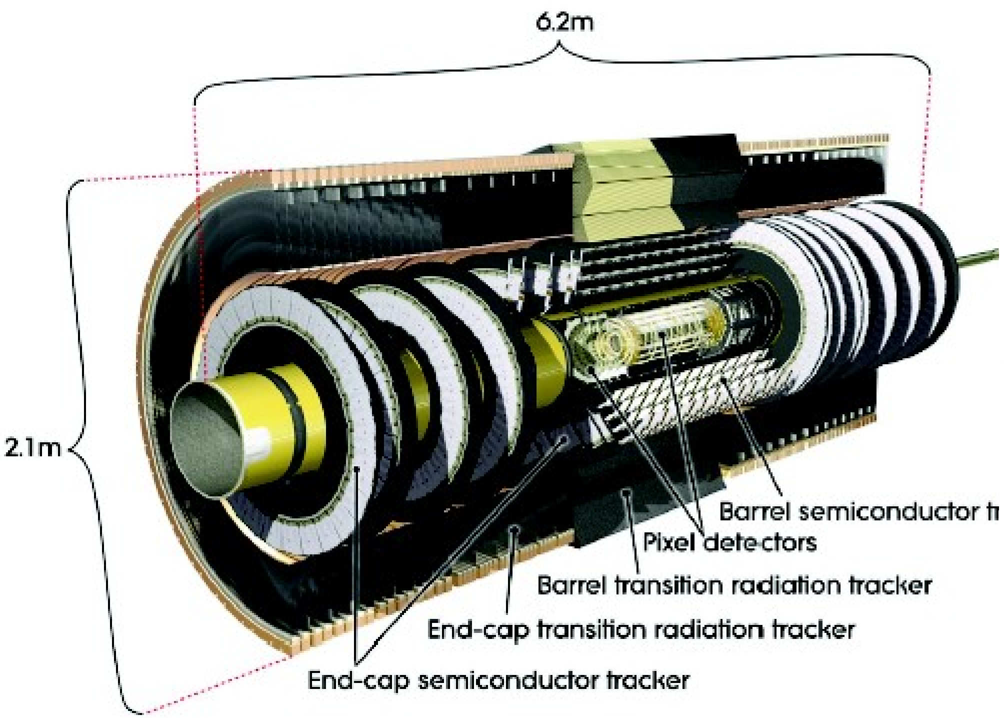

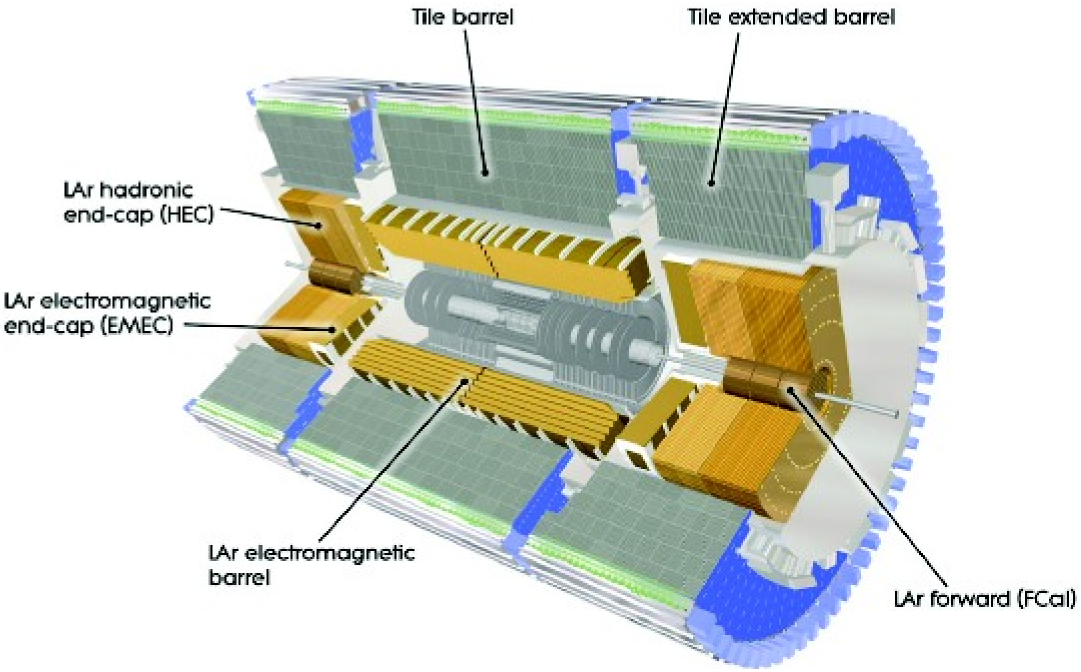

$$\frac{\sigma(p_T)}{p_T} = 0.036\% p_T + 1.3\%$$

$$\frac{\sigma(E)}{E} = \frac{50\%}{\sqrt{E}} + 3\%$$

Energy and time estimation in LAr calorimeter

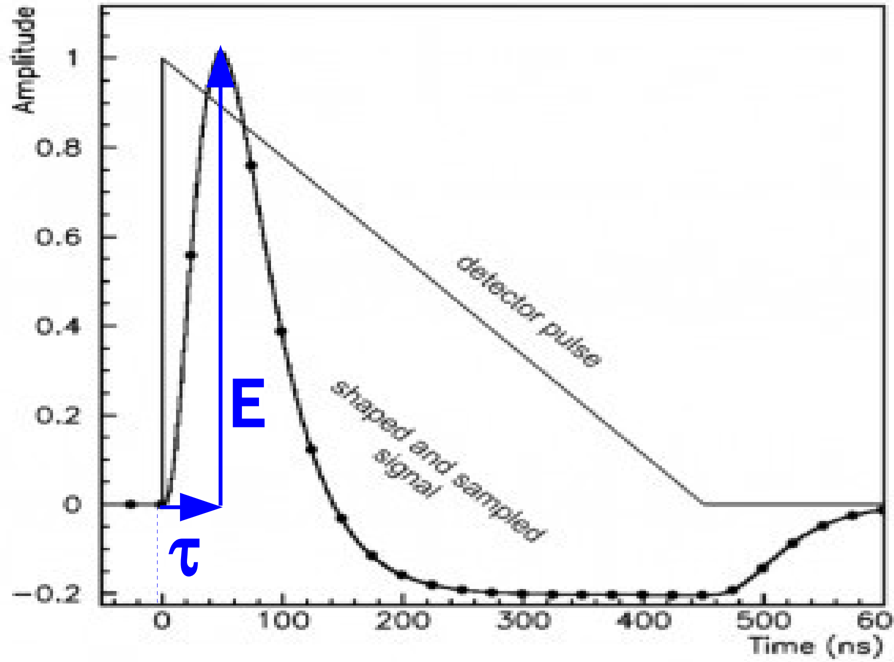

Relation between cluster energy and time and cell energy and time ?

- **Energy in a cluster is the sum of all its cells energies.**
- **Cluster time is τ of the most energetic cell.**

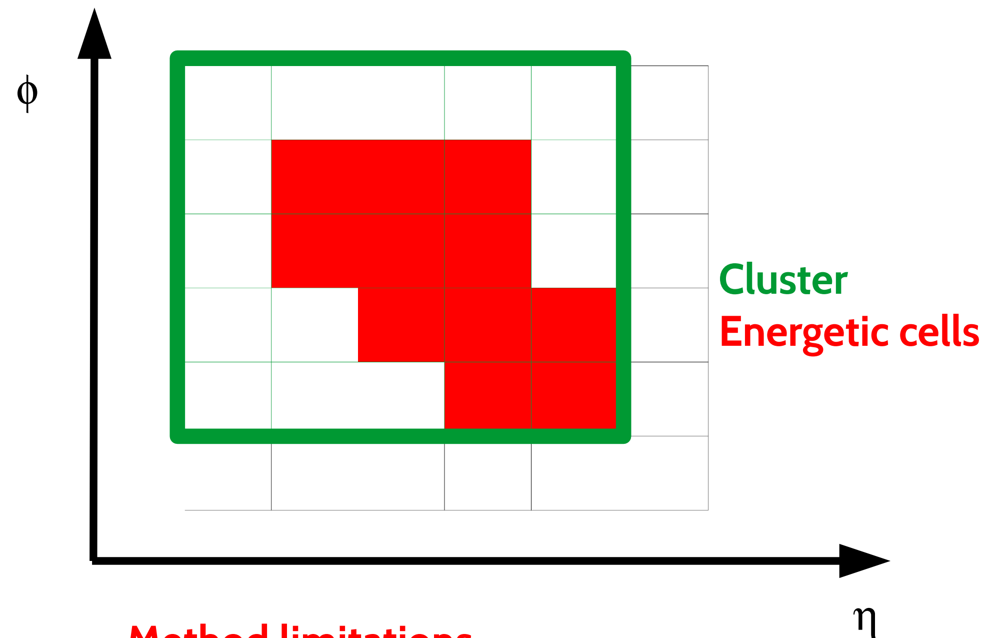

- In each cell, front end electronic takes 4 samples of the signal.
- An optimal filtering algorithm
  - OF coefficients are signal shape dependent.
- Signal peak   deposited energy.

$$\sum_{i=1}^{5} a_i S_i = E \qquad \sum_{i=1}^{5} b_i S_i = E\tau$$

Method limitations

- Cross-talk between cells limit timing resolution and energy precision.

$$E_{cell} = F_{\mu A \to MeV} F_{DAC \to \mu A} \frac{1}{\frac{M_{phys}}{M_{calib}}} \sum_{j=0}^{2} R_j \left(\sum_{i=0}^{4} a_i S_i \right)$$

LAr absorber

- Lead accordion-shaped absorbers
  - Two outer stainless-steel layers glued → mechanical rigidity.
  - Glass-fiber glue used.
- At |η| > 0.8, different absorber
  - More material → Lower sampling fraction in LAr .
  - Reduced lead thickness.

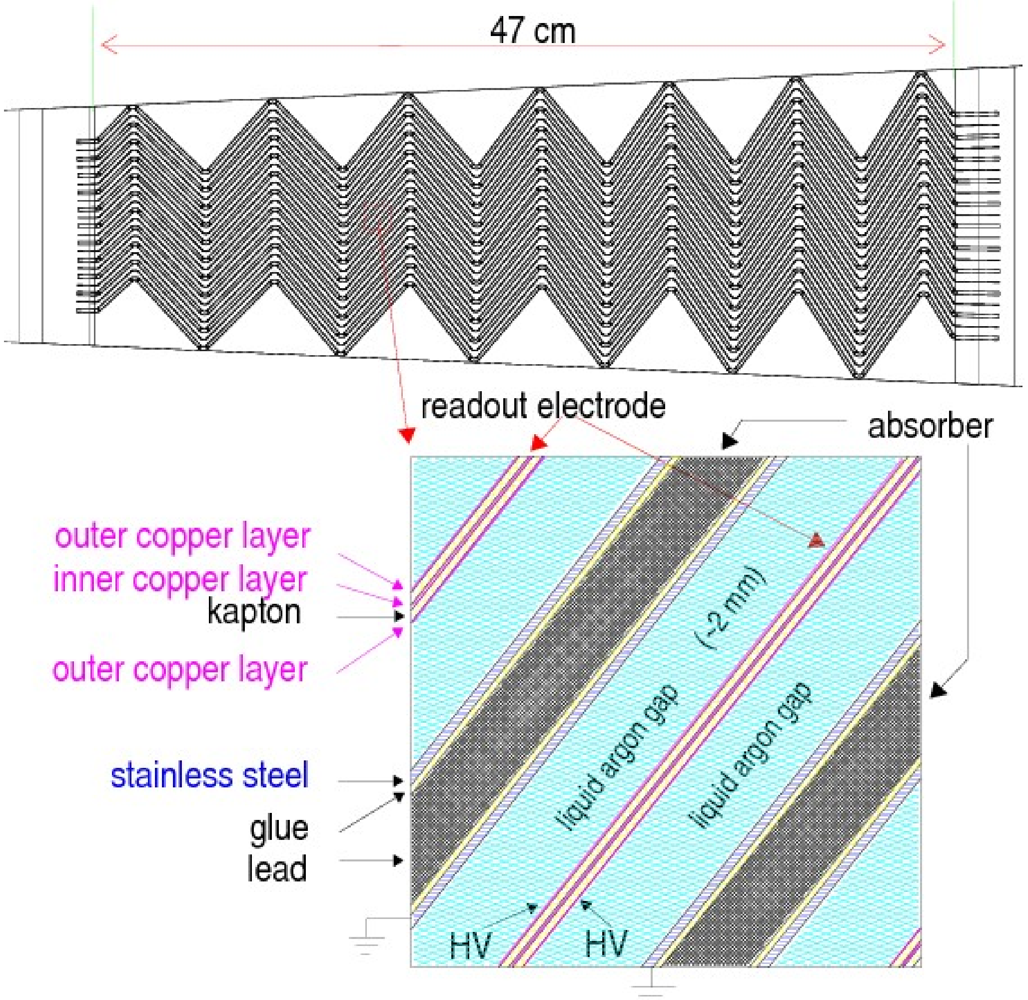

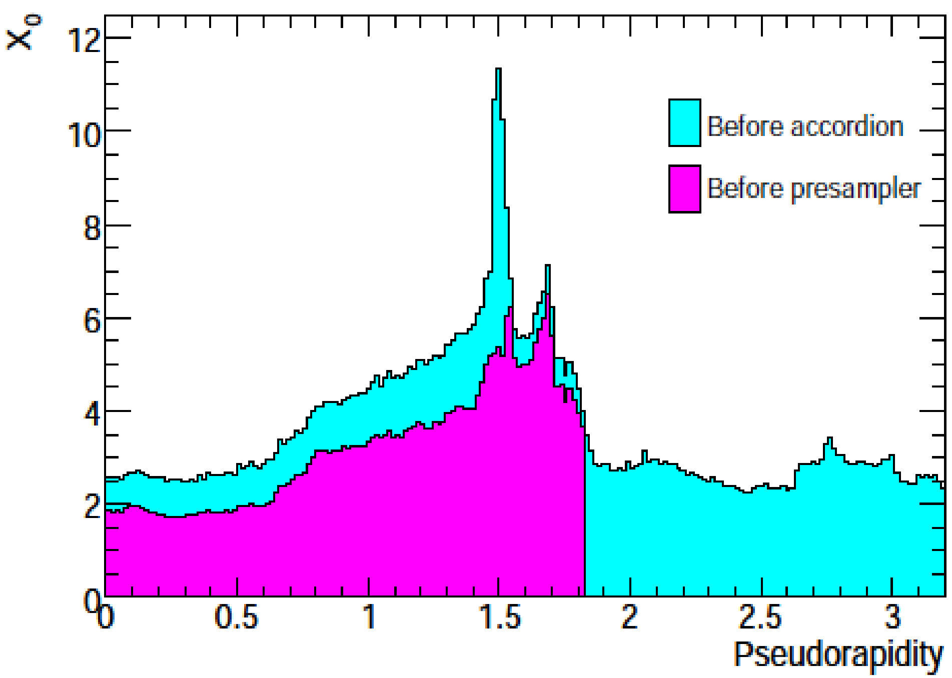

LAr read-out system

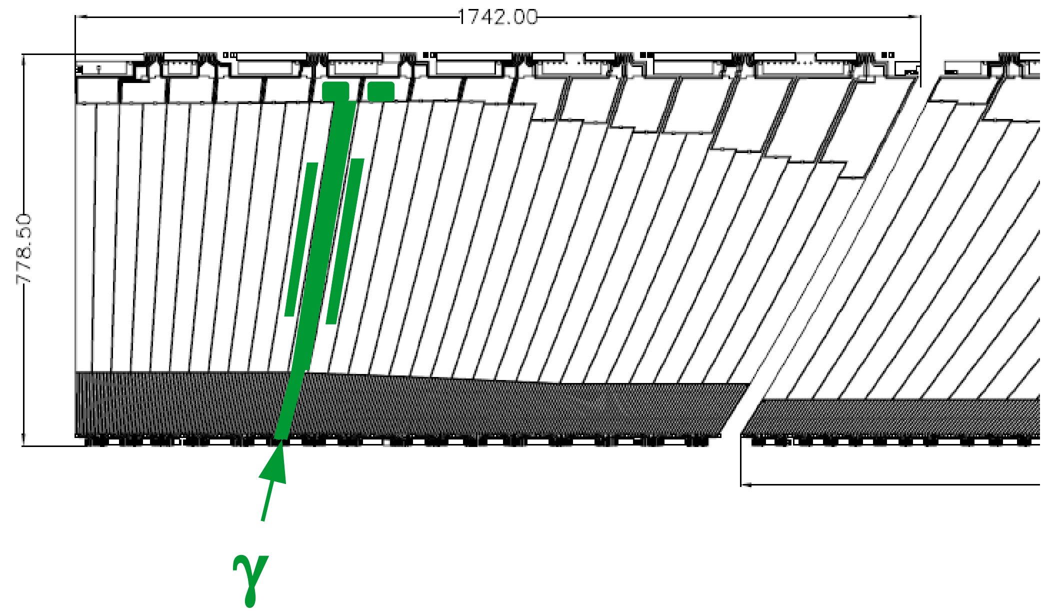

Electrode readout : capacitive coupling

Summing boards and mother boards (treat signals in $|\Delta\eta| \times |\Delta\phi| = 0.2 \times 0.2$)

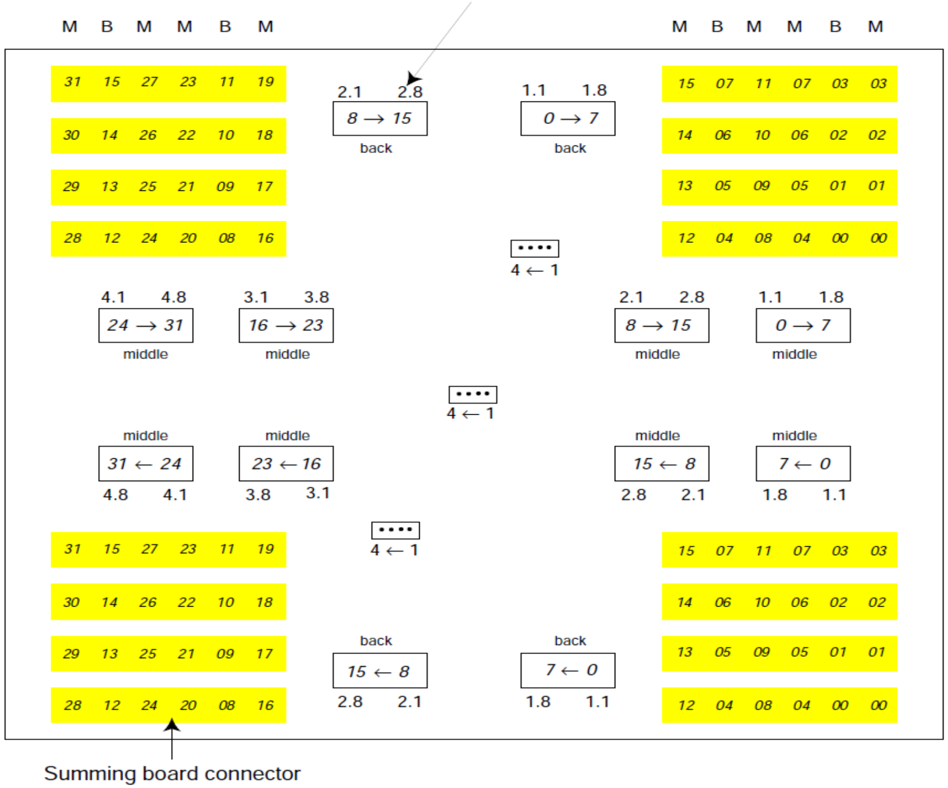

Front-end boards

Amplifier and shaper

SCA pipelines

L1 Calo Trigger

ROD

Optimal filtering coefficients

- Created in paper for optimal signal peak estimation against noise and pile-up in high interaction rate ionization detector.
- 5 samples (4 in Run II) of signals are retrieved.
- A factor to estimate the signal peak is applied, different for each sample (signal shape dependence)
- Calculated using Lagrange multipliers.
- Based on signal shape properties
  - Shape peak to 1.
  - $S_i = (Eg(t-\tau))_i = Eg_i(t) - E\tau g_i'$
  - Supposing noise suppression.
  - Minimize the variance of E and τ

$$\sum_{i=1}^{5} a_i S_i = E \qquad \sum_{i=1}^{5} b_i S_i = E\tau$$

$$\sum_{i=1}^{5} a_i g_i = 1 \quad ; \quad \sum_{i=1}^{5} a_i g_i' = 0$$

$$\sum_{i=1}^{5} b_i g_i = 0 \quad ; \quad \sum_{i=1}^{5} b_i g_i' = -1$$

- OFCs are predicted using delay calibration runs.
- In layer 1, cross-talk effect is quite big (~ 7% of total energy).
  - Signals are distorted due to it.
  - OFCs must be recalculated adding the neighbors cross-talk signals.
  - This is not done neither in the second nor third layers.
- Ramps are also recalculated since due to cross-talk in the strips, ADC peak was badly estimated and ADC → DAC conversion was not accurate.

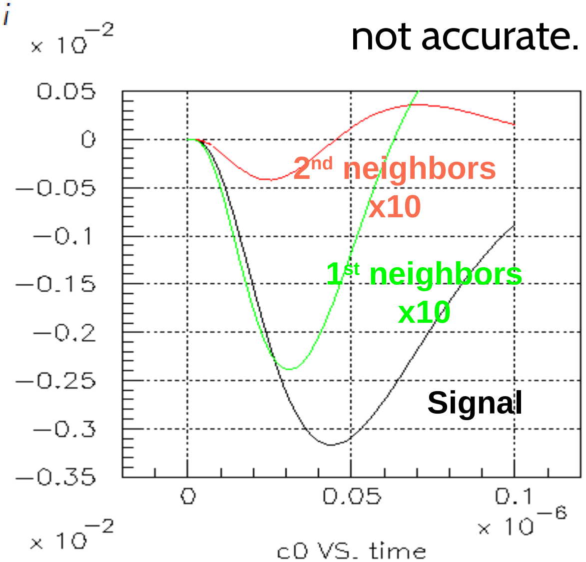

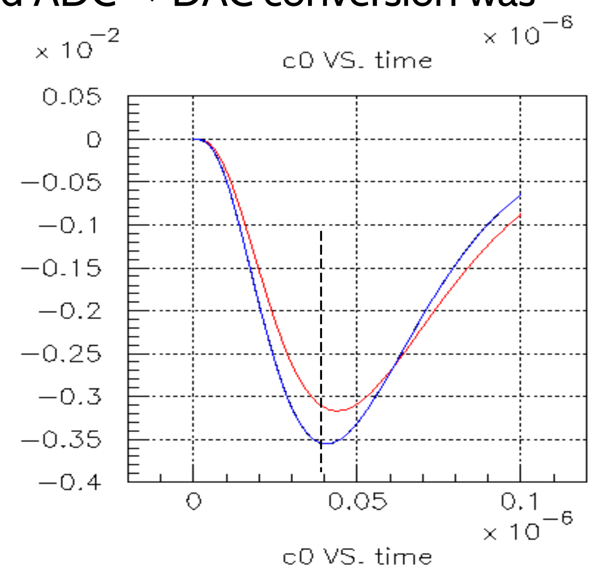

https://indico.cern.ch/event/423133/contribution/s1t5/attachments/893206/1257761/Calibration.ppt

Some CMS limits (monojets search)

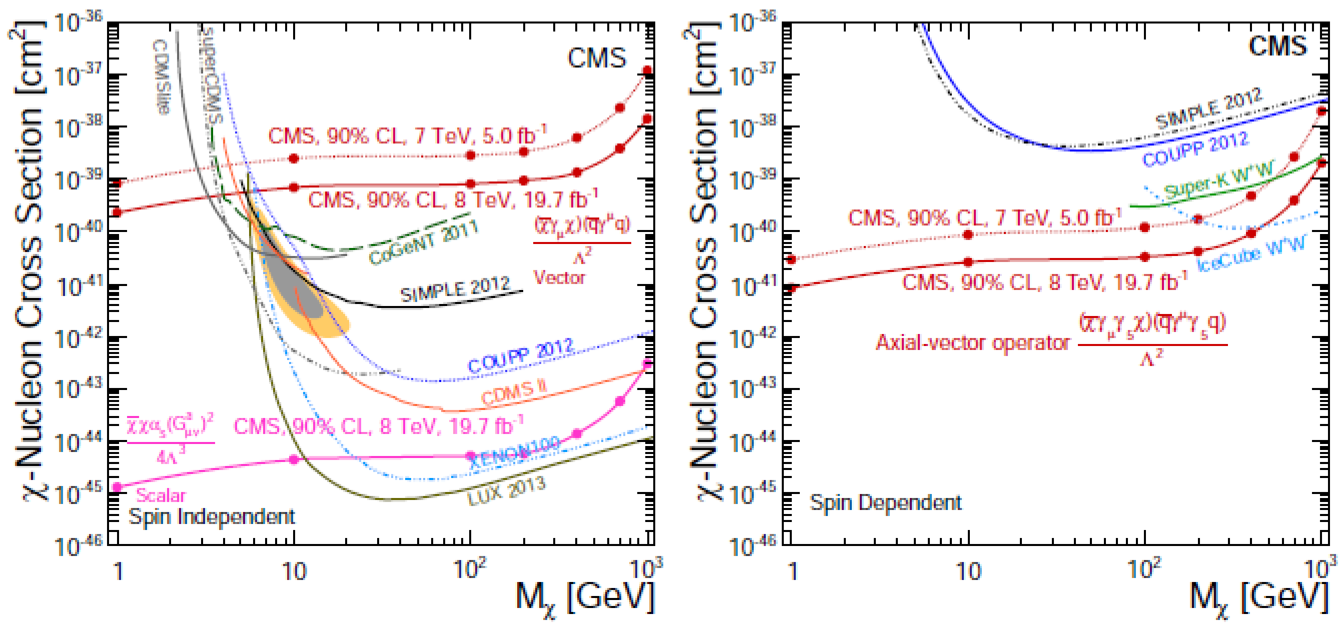

Figure 5: Upper limits on the DM-nucleon cross section, at 90% CL, plotted against DM particle mass and compared with previously published results. Left: limits for the vector and scalar operators from the previous CMS analysis [11], together with results from the CoGeNT [66], SIMPLE [67], COUPP [68], CDMS [69, 70], SuperCDMS [71], XENON100 [72], and LUX [73] collaborations. The solid and hatched yellow contours show the 68% and 90% CL contours respectively for a possible signal from CDMS [74]. Right: limits for the axial-vector operator from the previous CMS analysis [11], together with results from the SIMPLE [67], COUPP [68], Super-K [75], and IceCube [76] collaborations.

Some CMS limits (monojets search)

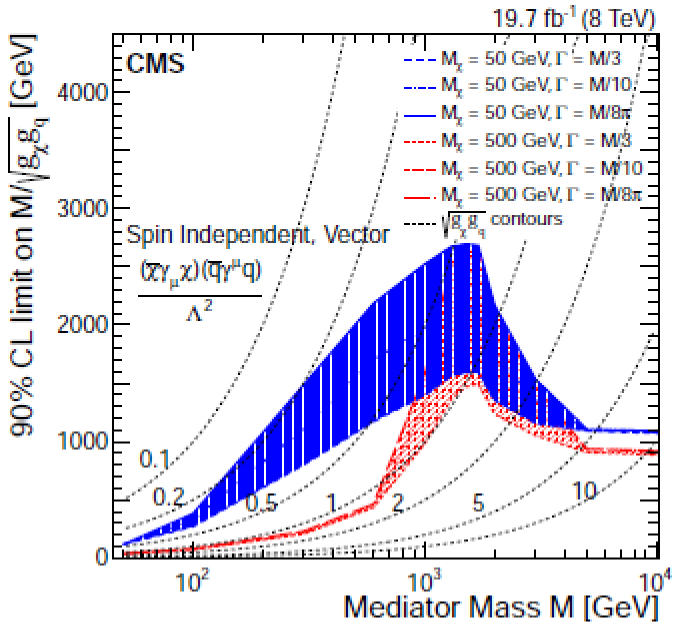

Figure 6: Observed limits on the mediator mass divided by coupling, $M/\sqrt{g_\chi g_q}$, as a function of the mass of the mediator, M, assuming vector interactions and a dark matter mass of 50 GeV (blue, filled) and 500 GeV (red, hatched). The width, Γ, of the mediator is varied between $M/3$ and $M/8\pi$. The dashed lines show contours of constant coupling $\sqrt{g_\chi g_q}$.

Some CMS limits (Z' resonances decaying into HZ)

$\sigma_{Z'}$ depends on Lagrangian term : $g_q \bar{q} \gamma^{\mu} q Z'_{\mu}$

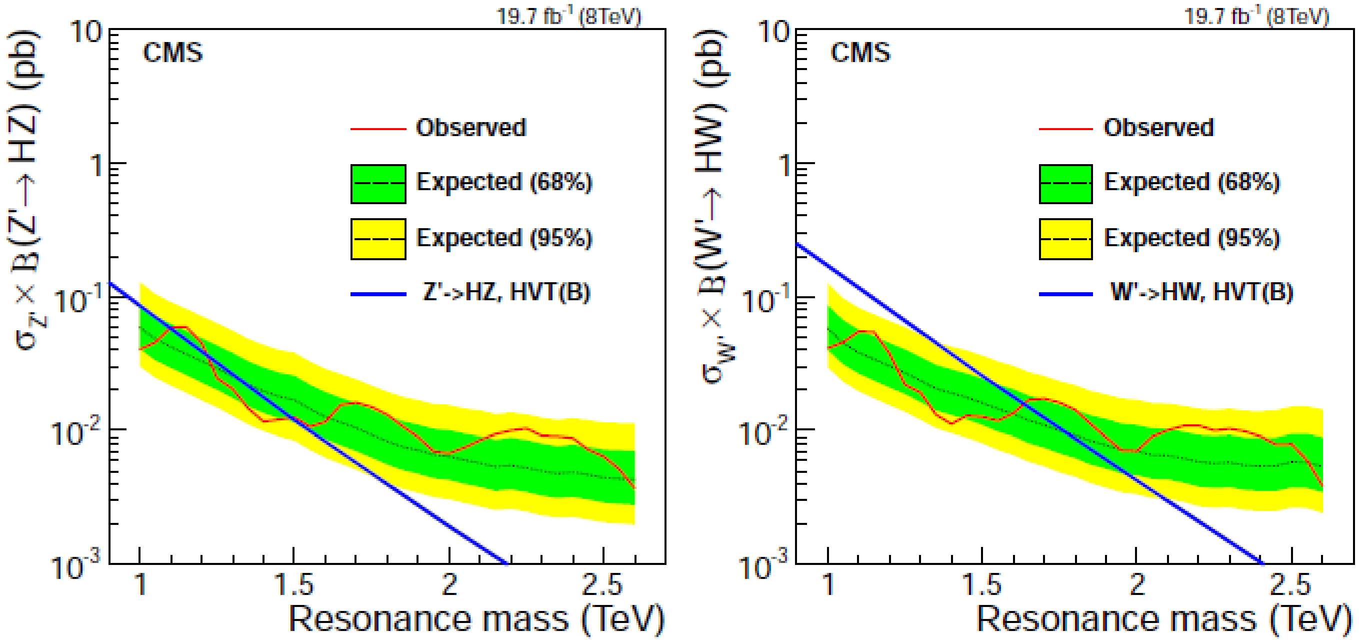

Figure 9: Expected and observed upper limits on the production cross sections for $Z' \to HZ$ (left) and $W' \to HW$ (right), including all five decay categories. Branching fractions of H and V decays have been taken into account. The theoretical predictions of the HVT model scenario B are also shown.